factor values above 100 are detected.

(2) Line 400W

Same as the Line 0, the detected resistivity values show low values, and near the surface, resistivity values lower than 10 Ohm-m are detected.

The chargeability values show in general values lower than 5 mV/V.

The high metal factor values detected are, in general, the results reflected by the low resistivity values. The low resistivity values distributed at shallow depths correspond to the high metal values detected close to the surface.

4-10 Daris Area

4-10-1 Lines location

In this area, 15 IP lines were located along the N10E direction, making a total of 44.0 km. The initial schedule consisted only of 9 lines of 2 km each and centered along the gossan area, however, since the partial chargeability results of the survey showed some promising area to the north and north west, the lines were expanded to the north about 1.6 km and added lines to the west. The locations of the lines are indicated in Fig. II-4-40.

4-10-2 Results

Regarding the apparent resistivity distribution of the area, in can generally be mentioned that from south to north, it can be seen a distribution of relatively low values of less than 50 Ohm-m, followed by a high distribution zone of less than 100 Ohm-m, then a low resistivity distribution, ad finally followed by a medium resistivity distribution zone between 50 to 100 Ohm-m. These low and high distributions present a NW-SE trending at all depths as seen in all the plan maps from n=1 to 4. In the gossan area (station 10 of line 0) as well as its surroundings, the above mentioned distributions can be seen only at the depths of n=1 (100m) and n=2(100 to 150m) a low apparent resistivity zone of less than 50 Ohm-m, but specially low at the stations 10 of the lines 0 and 200W.

The chargeability values show in general the same correlation observed with the resistivity, for instance, in the central zone where high resistivity values were seen, relatively high chargeability values above 10 Ohm-m are seen. In the southern zone of low apparent resistivity values, also low values of less than 6 mV/V are seen, however, the south part of the area which shows low resistivity values shows high chargeability values. Moreover, the extracted magnetic anomalies from the acromagnetic survey, which runs parallel to the boundary zone of high apparent resistivity values (high chargeabilities) and the south zone of low apparent resistivity

(low chargeability) crosses the central part of the gossan zone.

The metal factor shows almost the same pattern than the apparent resistivity, showing high values in places where low resistivities are found. High values above 30 were especially detected in the gossan (station 10 of line 0) as well as the surrounding zones, and the surroundings of the following stations: station 4 line 600E, station 5 line 600W, station 19 of line 400W, the north part of the area (station 28 of line 400W to station 20 line 1000E) as well as station 13 of line 800E. Among them the gossan (station 10 of line 0) and surroundings, station 19 of line 400W and surroundins, as well as the north part of the area (from station 28 of line 400W to st.20 of line 1000E) are places of medium of high chargeabilities that are likely to be associated to mineralization.

4-10-3 2-D analysis

(1) Line 0

From the central part of this line towards the south, relatively low resistivity values are distributed at the shallow part and high resistivity at the deep parts. Specially, the stations 10 where the gossan is located and the station 4 show lower resistivity values at shallow depth. Moreover, a low resistivity distribution is seen trending from the shallow part of the station 27 to the deep part of the station 29.

Regarding the chargeability, from the central part of the line to the south, it can be seen a correspondence between the chargeabilities and resistivities and therefore, in places of high resistivity are found also high chargeabilities. From station 29 at shallow depth to station 31 at deep levels can be seen a trending of relatively low resistivity values corresponding to high chargeability values.

In relation to the metal factors, the low resistivity distribution are also in agreement with the metal factor results, and in this regards, it can be said that the above mentioned zone of low resistivity from station 27 at shallow part to 29 at deep part show high metal factor values above 100.

(2) Line 200W

The apparent ressitivity distribution shows almost same pattern as the previous line 0, showing from the central part to the south, low apparent resistivity at shallow depth, and high resistivity at deep parts. To the north part of this line from stations 28 to 30 can be seen a low resistivity distribution at deep levels and extended to the shallow depth of the station 25.

Regarding the chargeability, it shows almost same pattern as line 0. showing high values at the deep parts of the stations 19 to 21. Moreover, from the shallow part of station 29 to the deep portion of station 32, it can be seen a distribution of high metal factor values.

In relation to the metal factor, from the shallow depth of station 28 to the deep part of station 30, it can be seen metal factor values higher than 80 in agreement with the above mentioned low resistivity distribution.

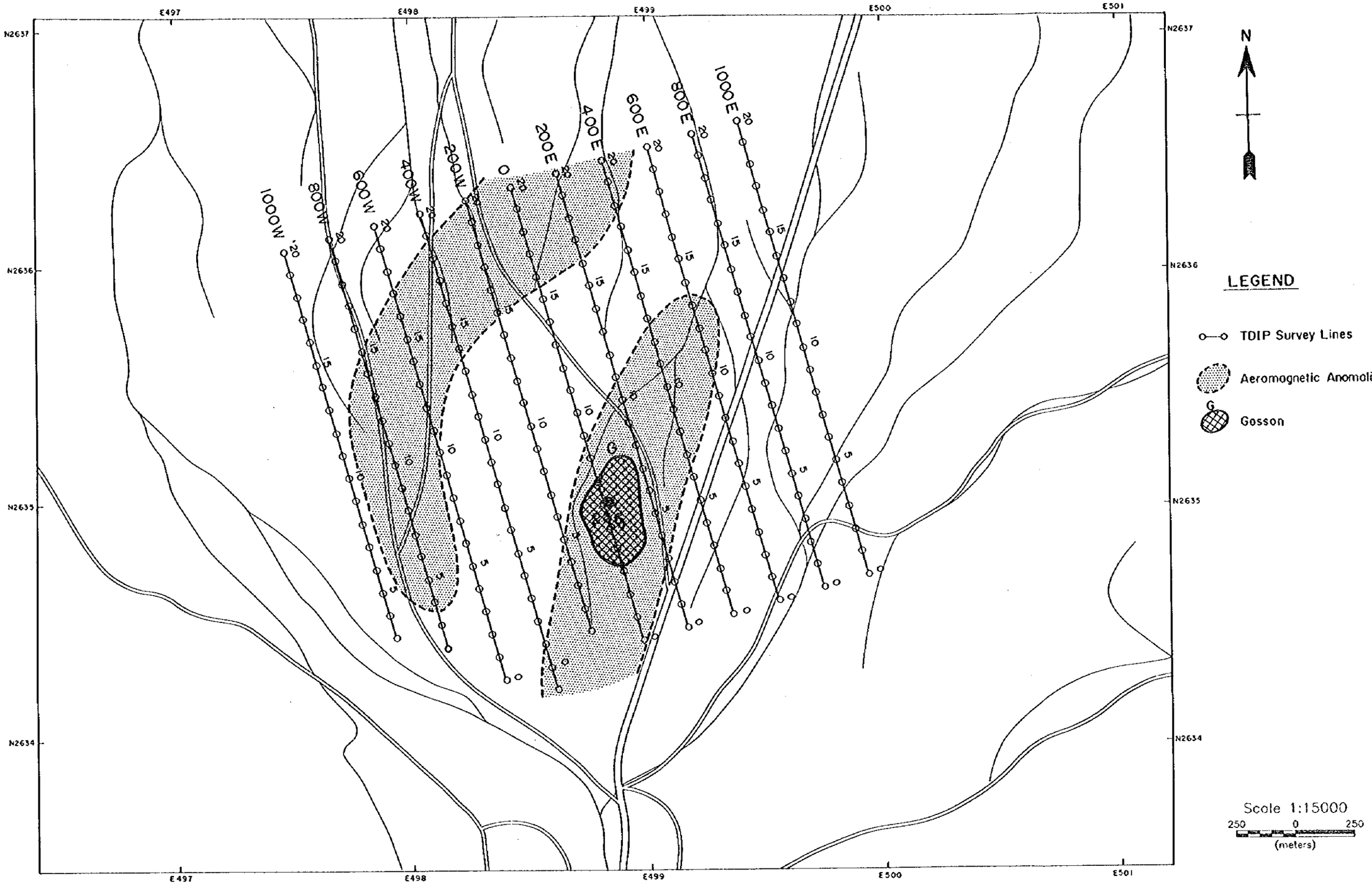

Fig. II-4-4 IP line locations in Ghuzayn Gossan area

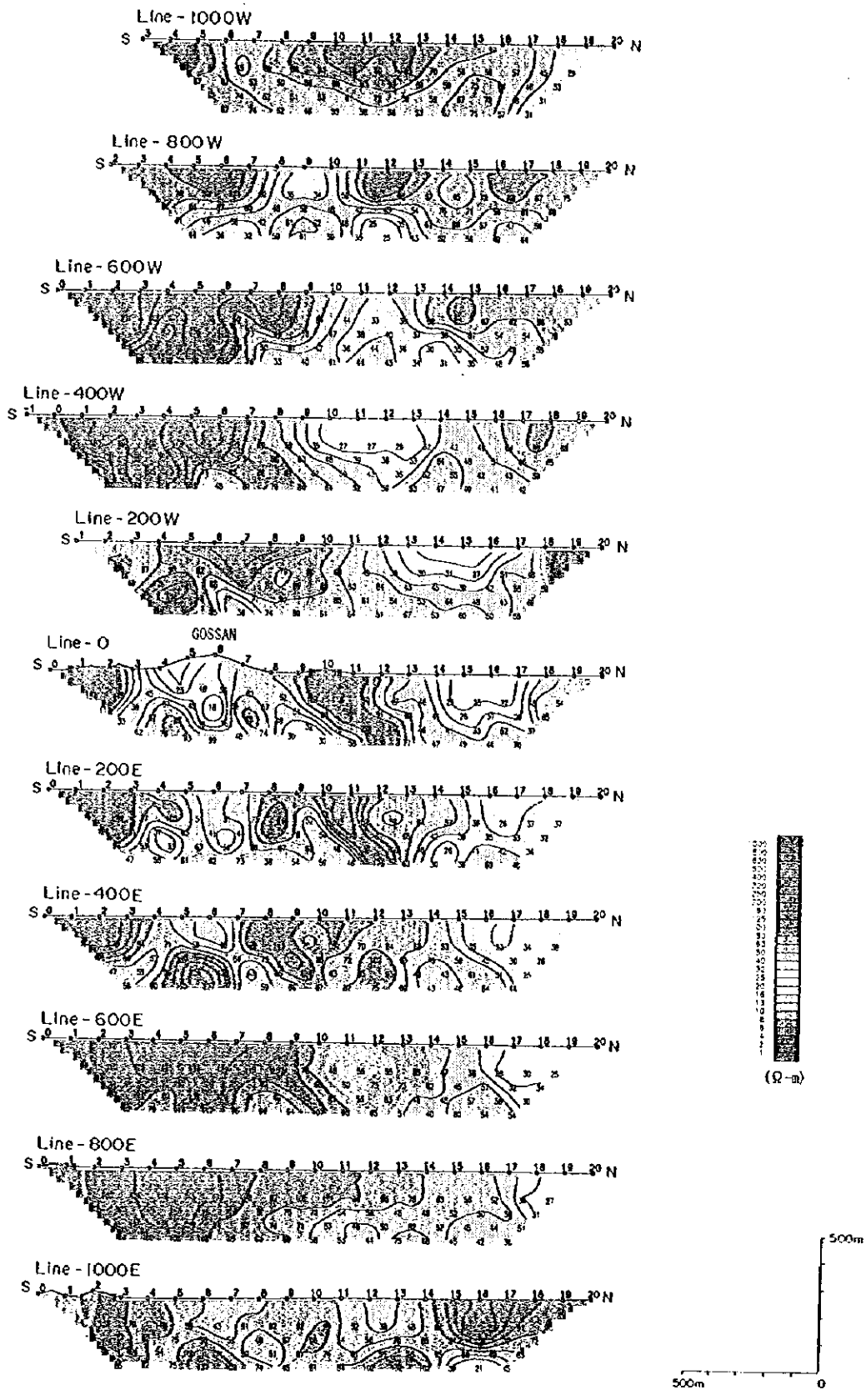

Fig. II-4-5 Apparent resistivity pseudo-sections in Ghuzayn Gossan area

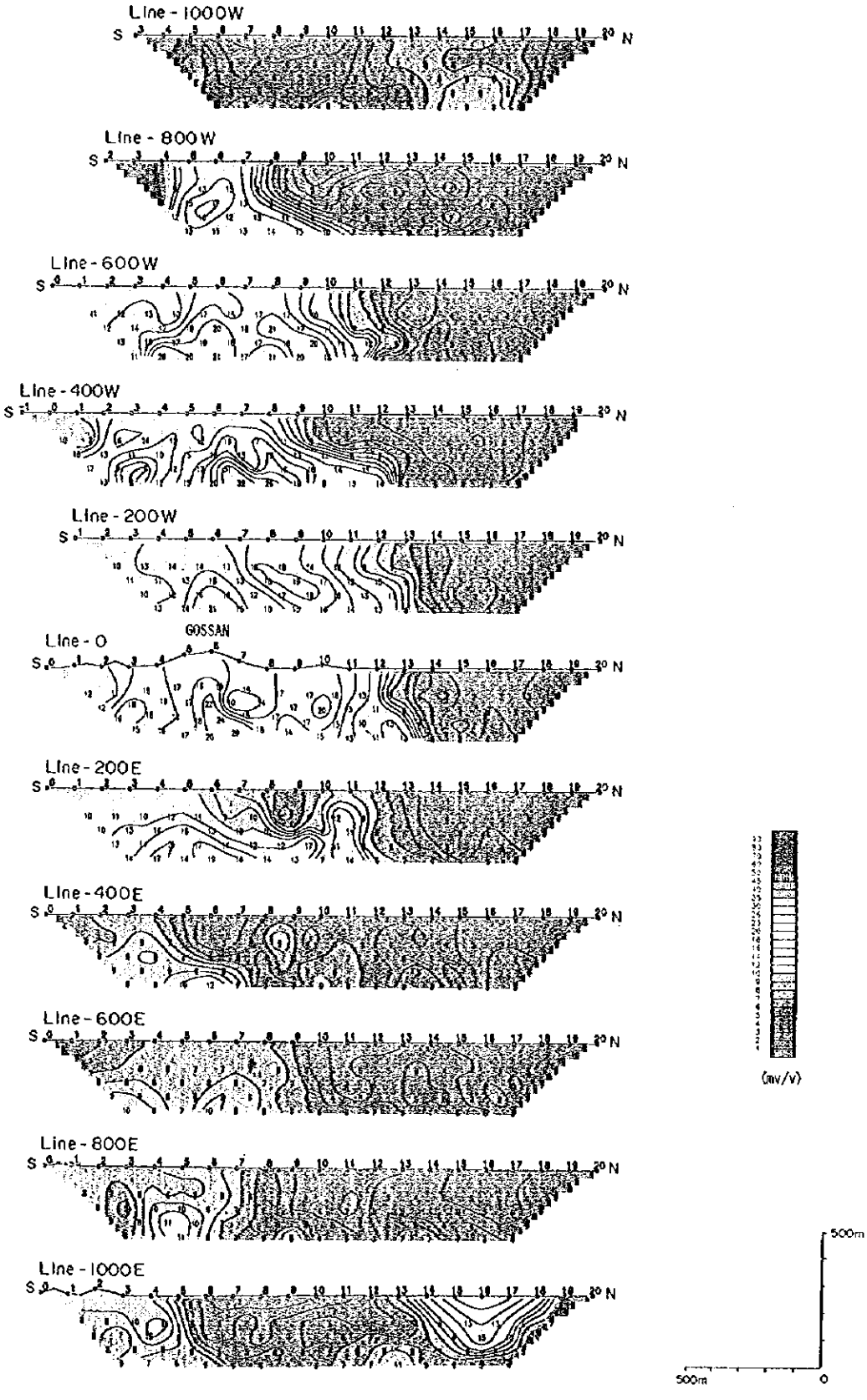

Fig. II -4-6 Chargeability pseudo-sections in Ghuzayn Gossan area

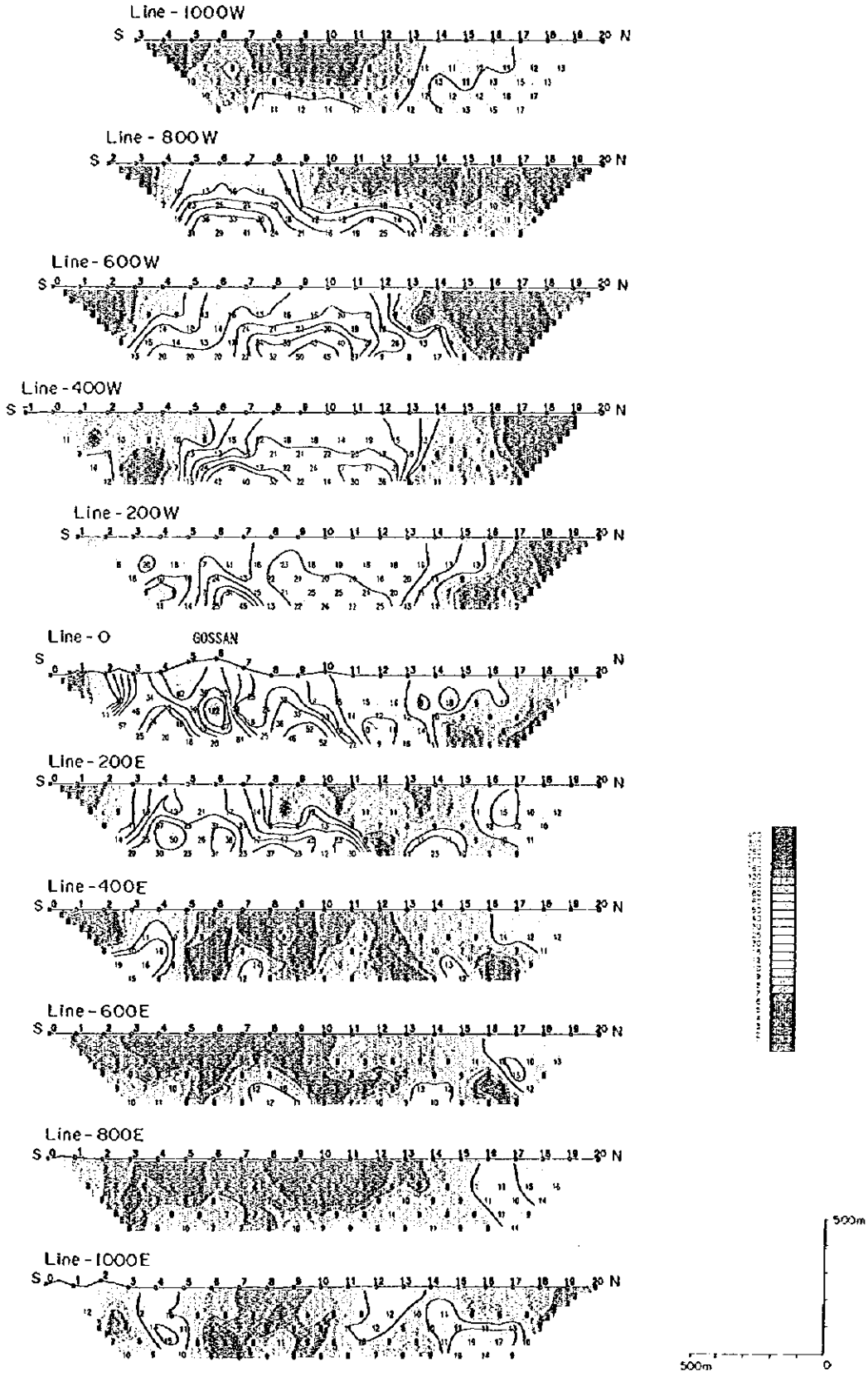

Fig. II -4-7 Metal factor pseudo-sections in Ghuzayn Gossan area

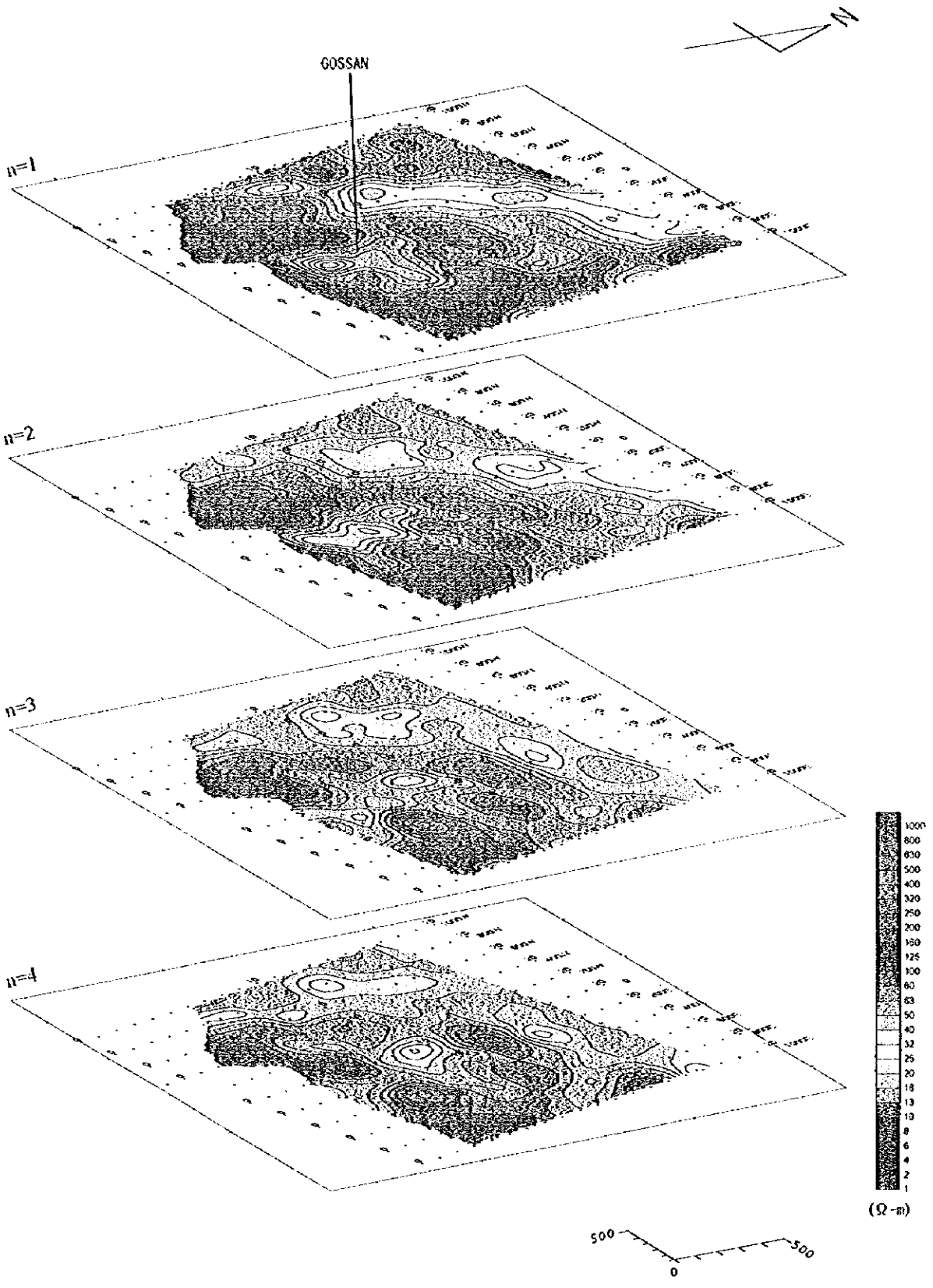

Fig. II -4-8 Apparent resistivity plan map in Ghuzayn Gossan area

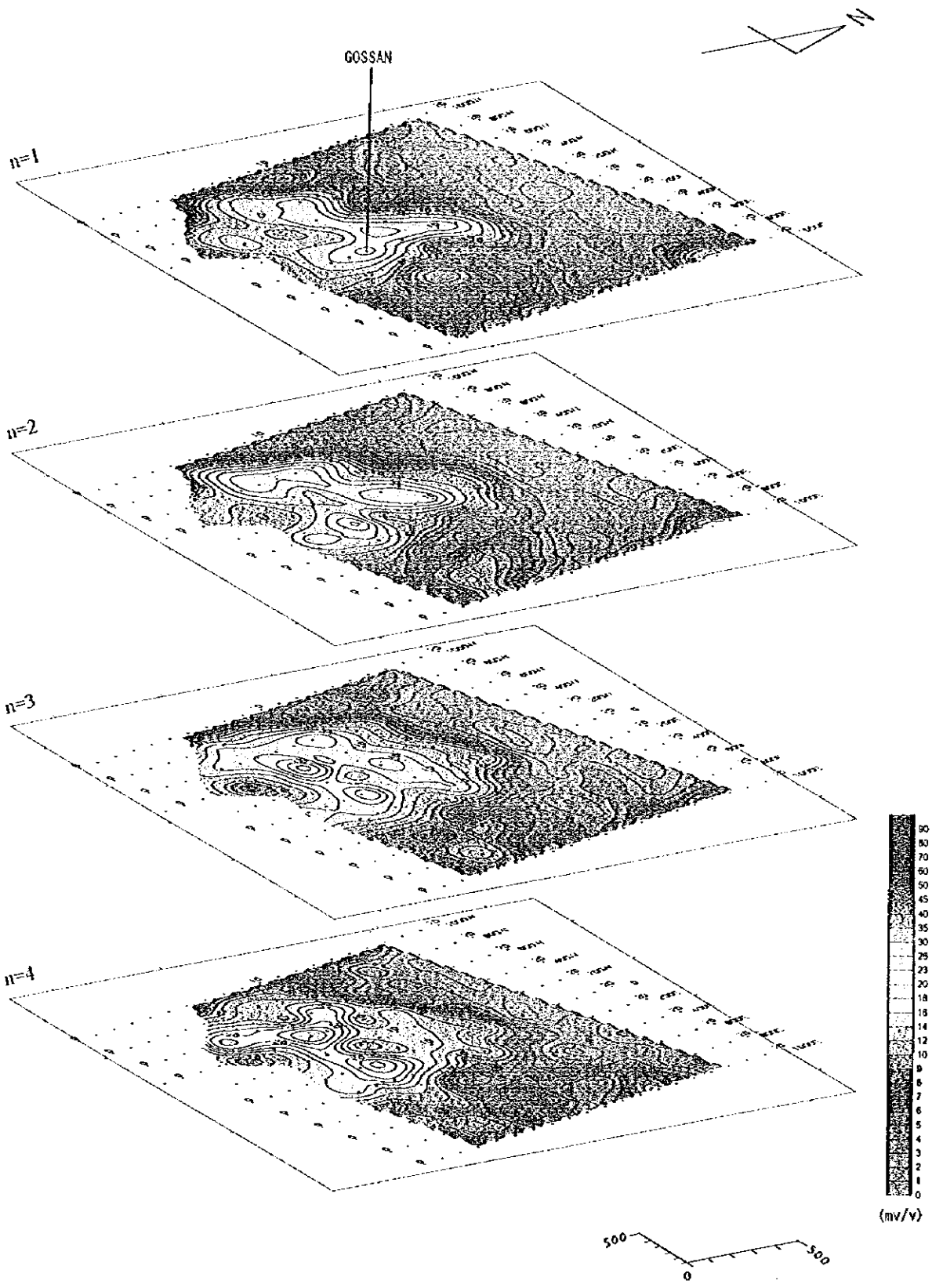

Fig. II -4-9 Chargeability plan map in Ghuzayn Gossan area

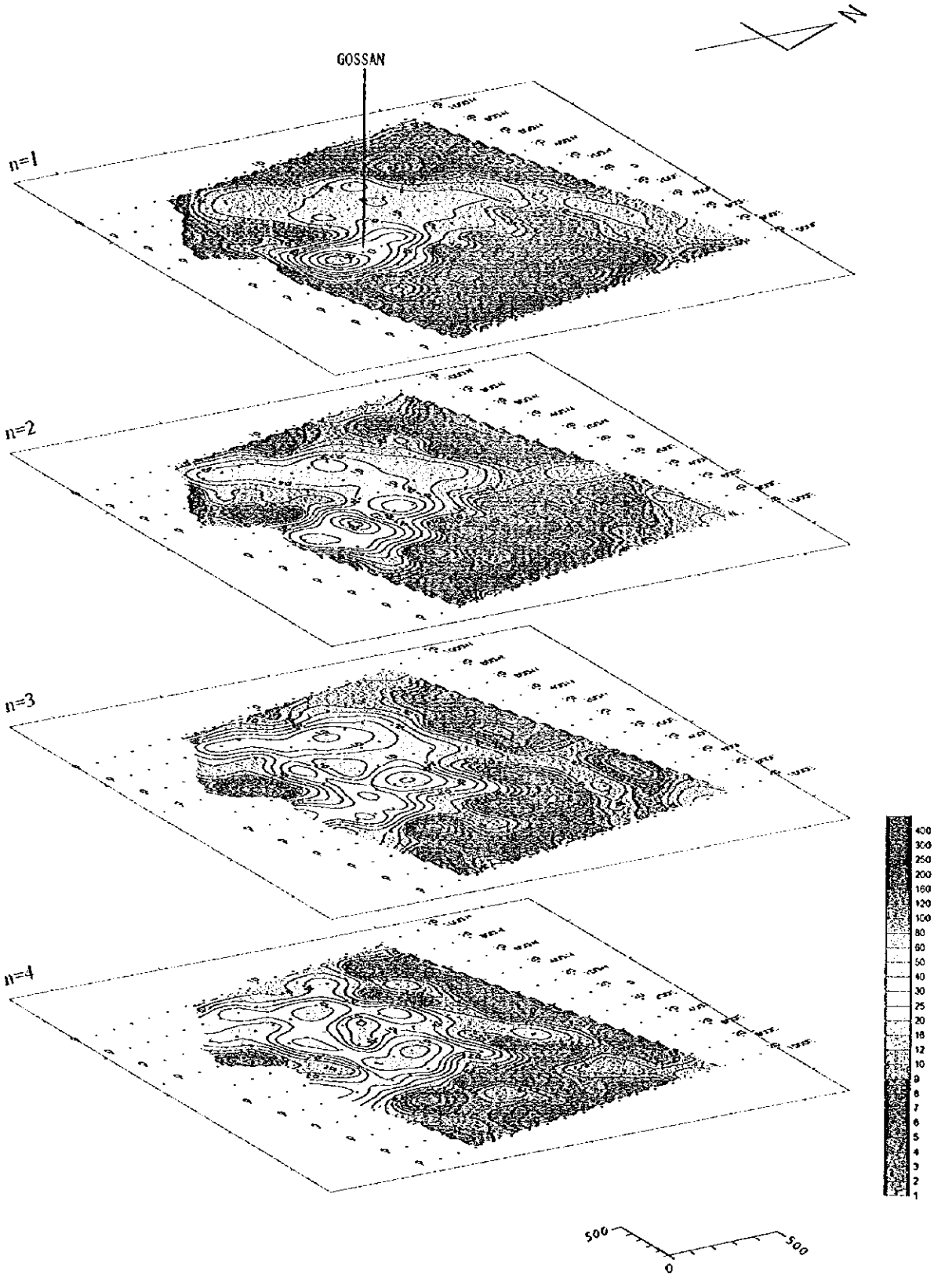

Fig. II -4-10 Metal factor plan map in Ghuzayn Gossan area area

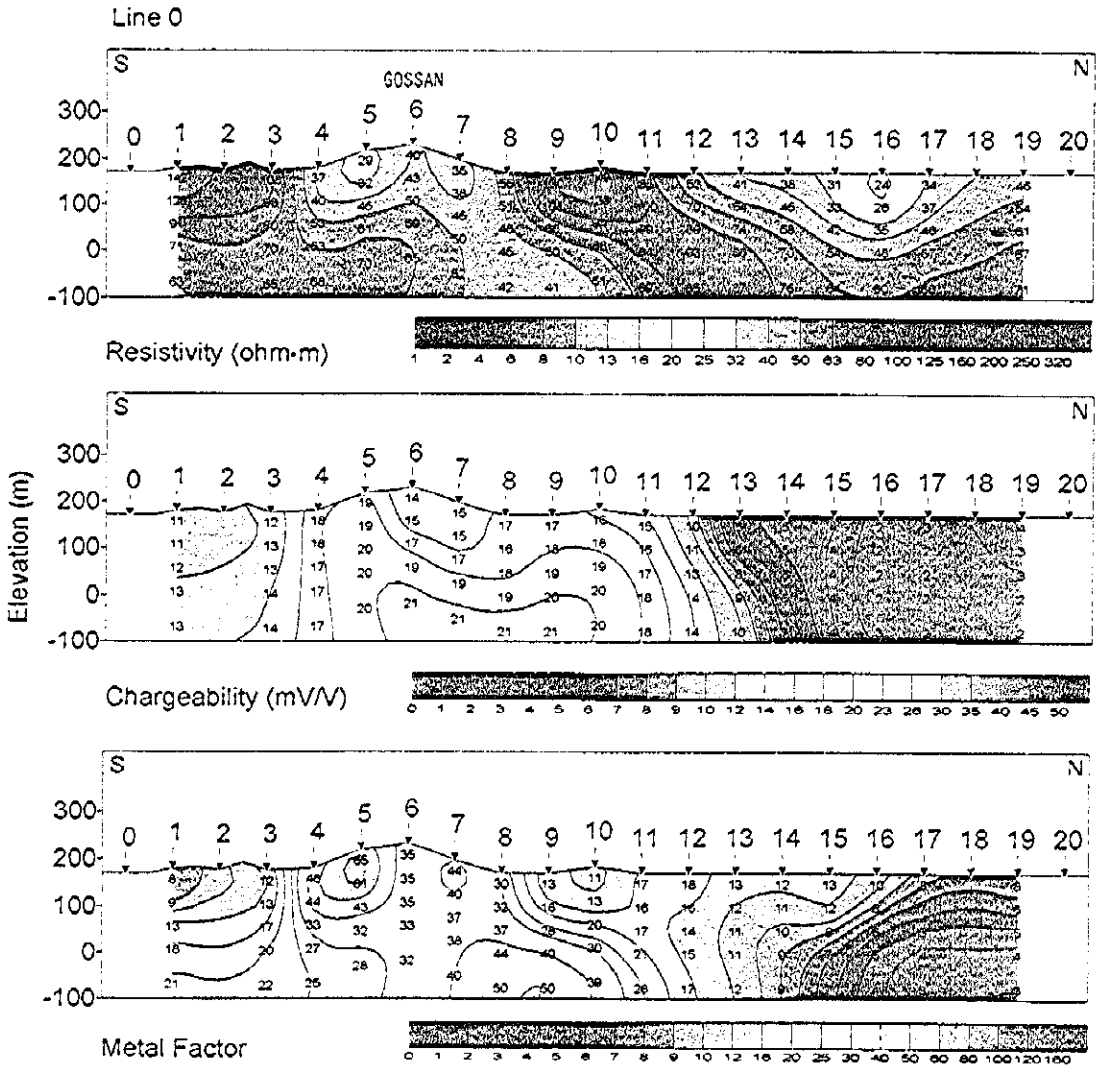

Fig. II-4-11 Results of model simulation in Ghuzayn Gossan area(1)

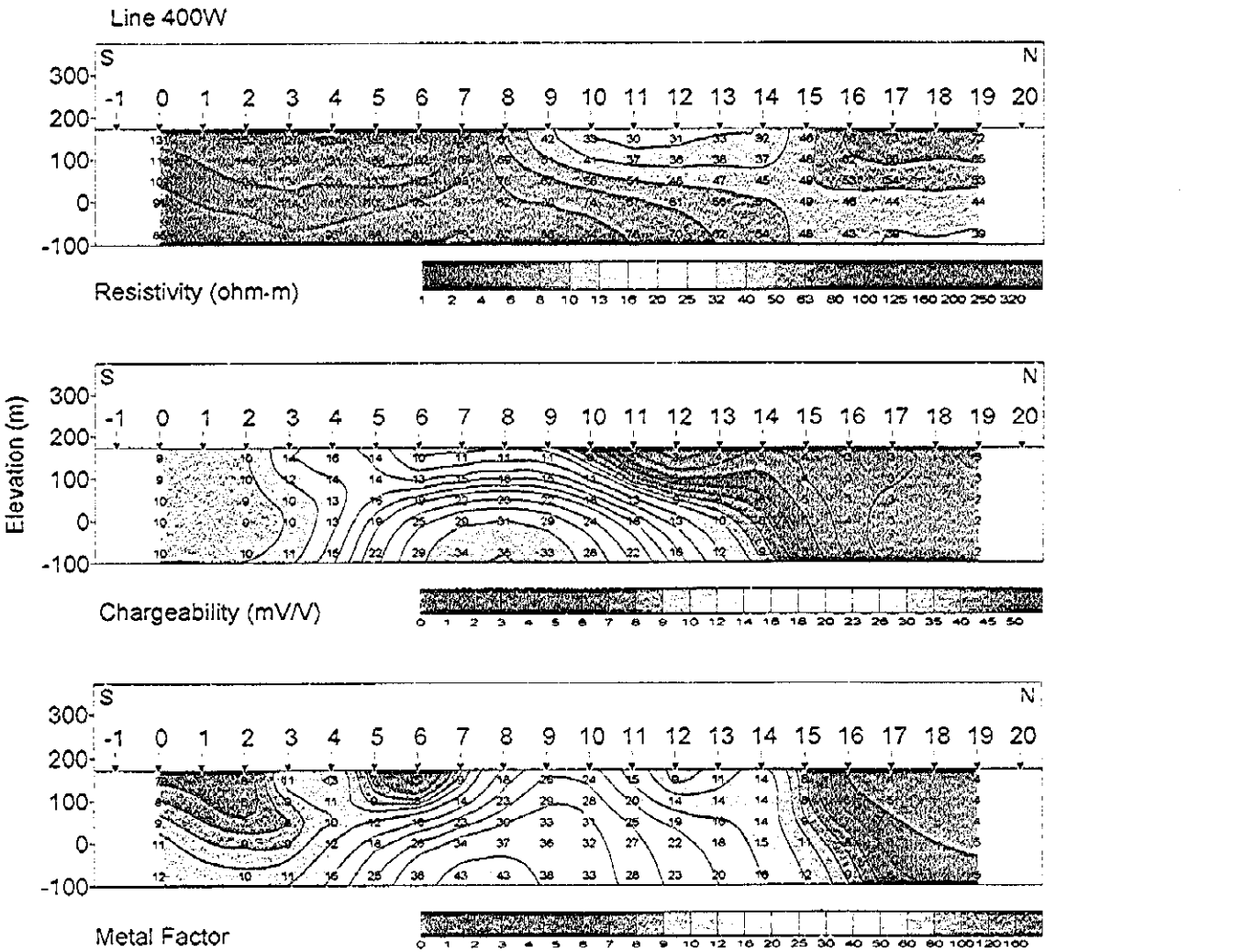

Fig. II -4-12 Results of model simulation in Ghuzayn Gossan area(2)

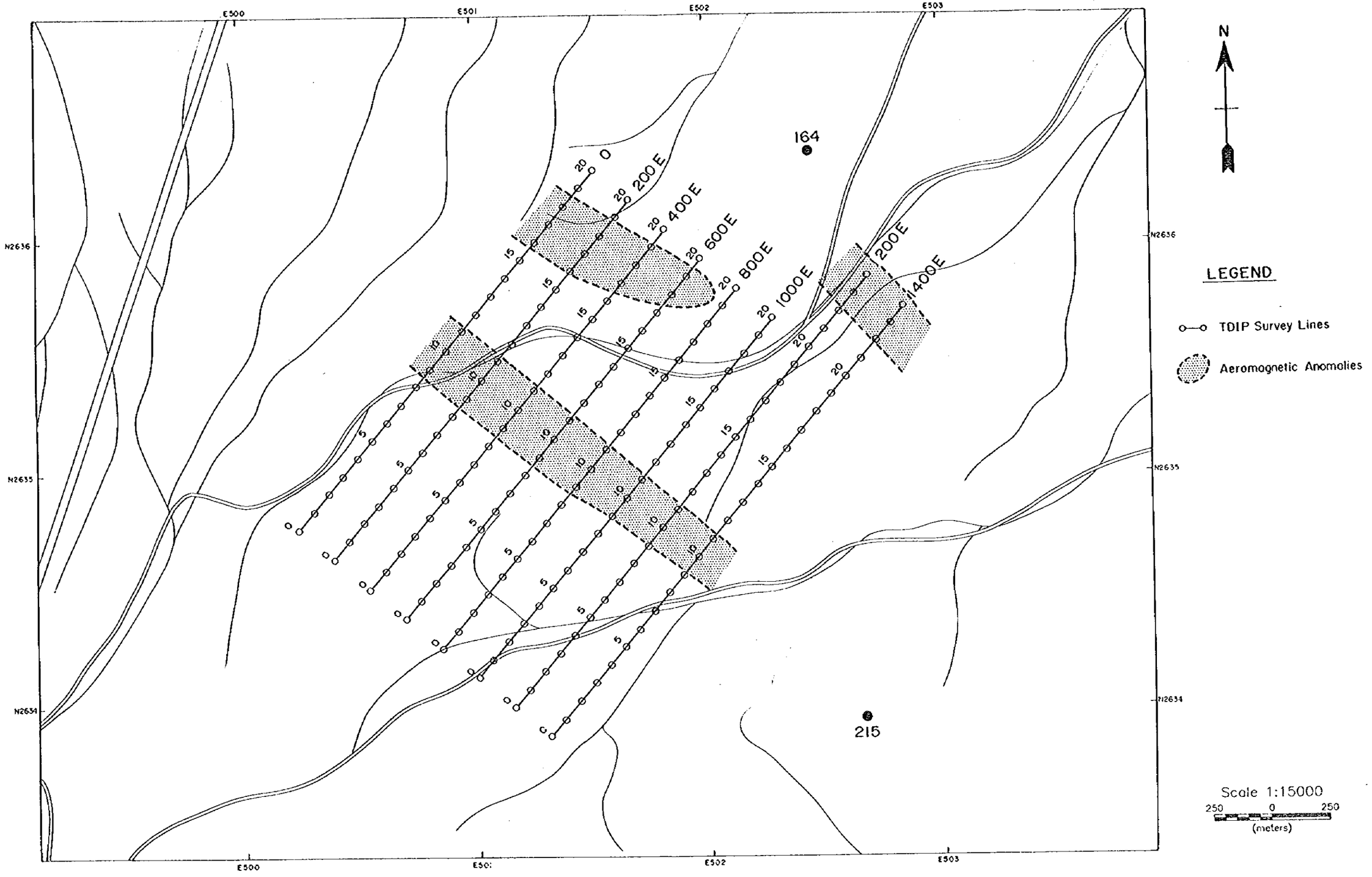

Fig. II-4-13 IP line locations in Ghuzayn East area

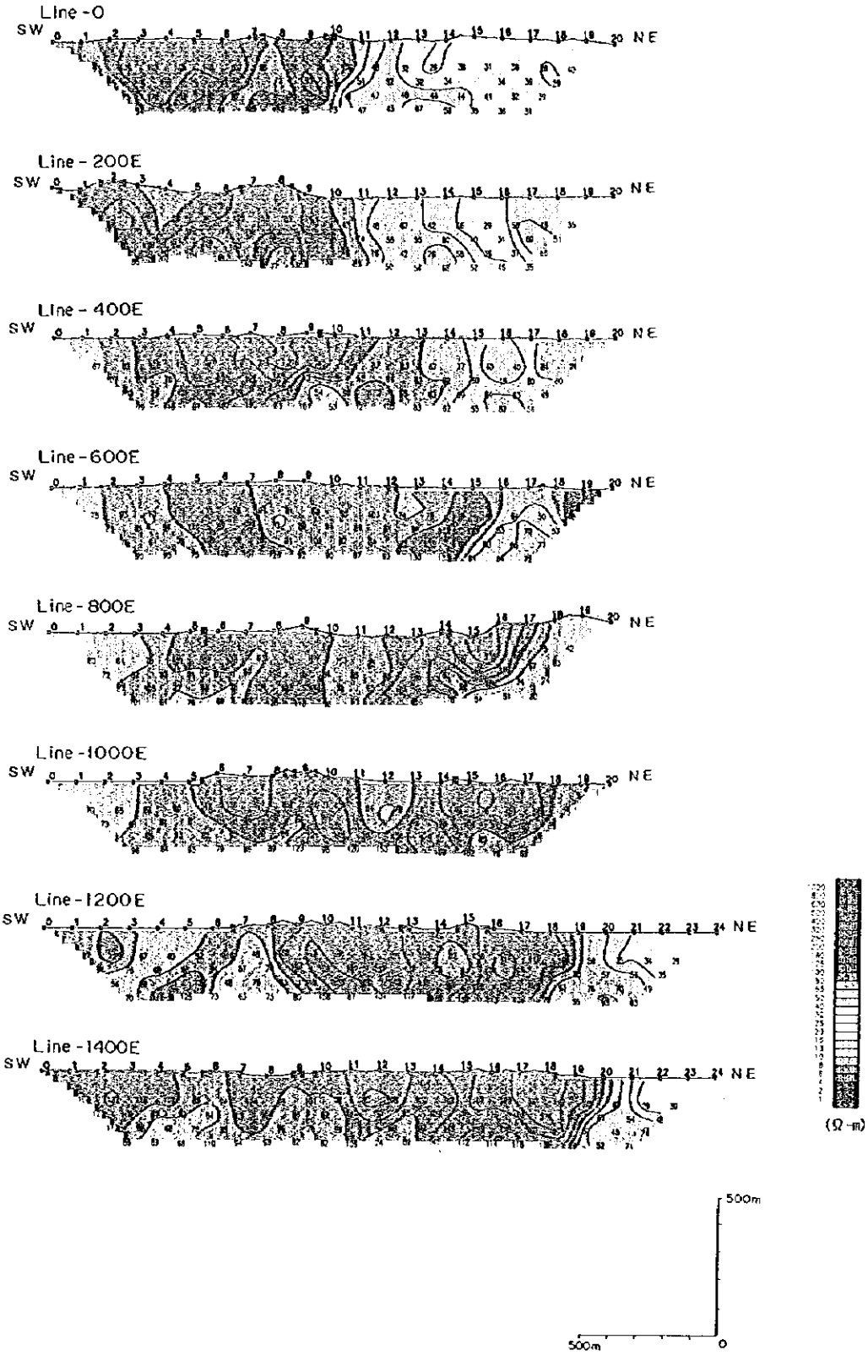

Fig. II -4-14 Apparent resistivity pseudo-sections in Ghuzayn East area

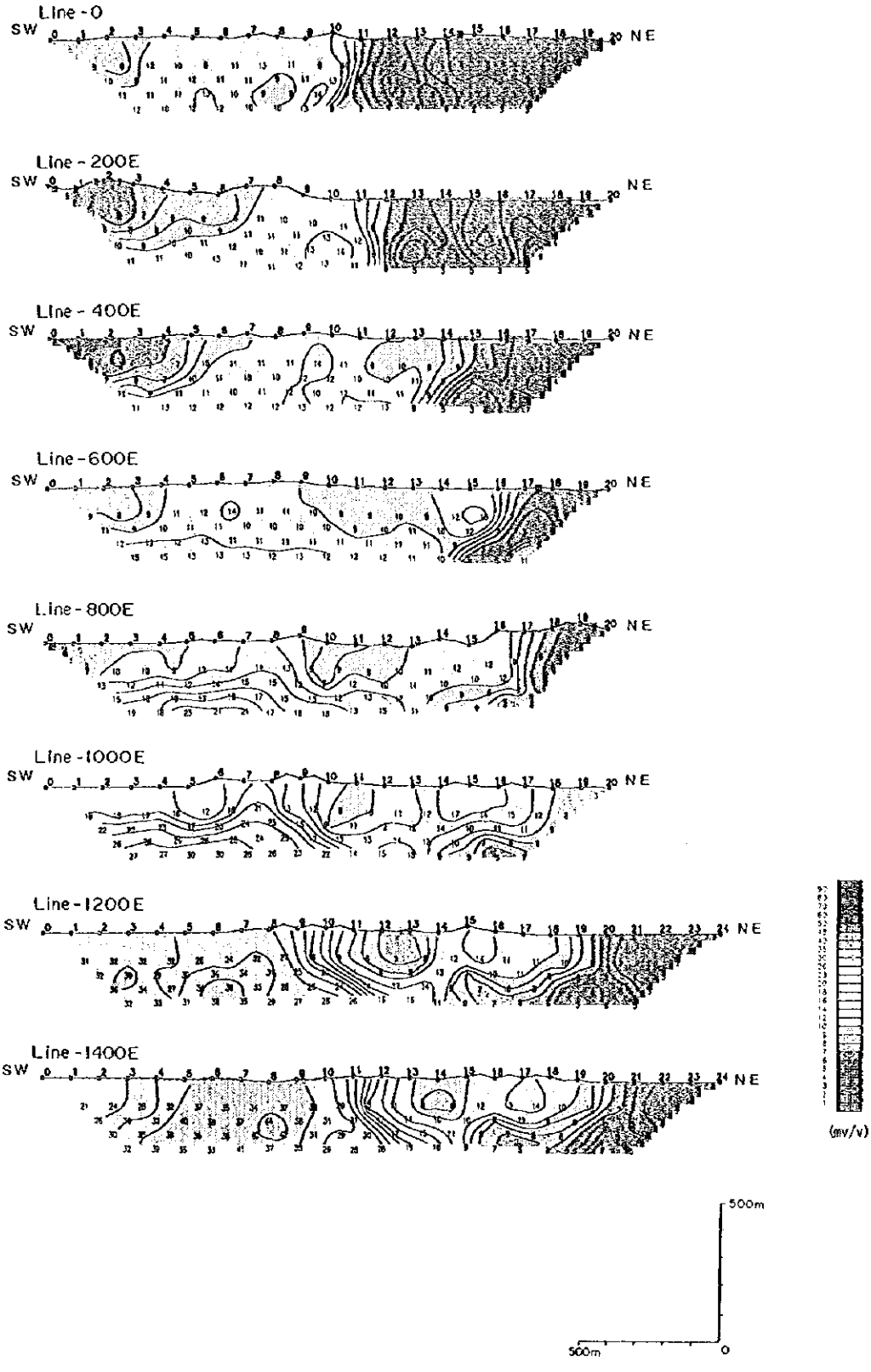

Fig. II-4-15 Chargeability pseudo-sections in Ghuzayn East area

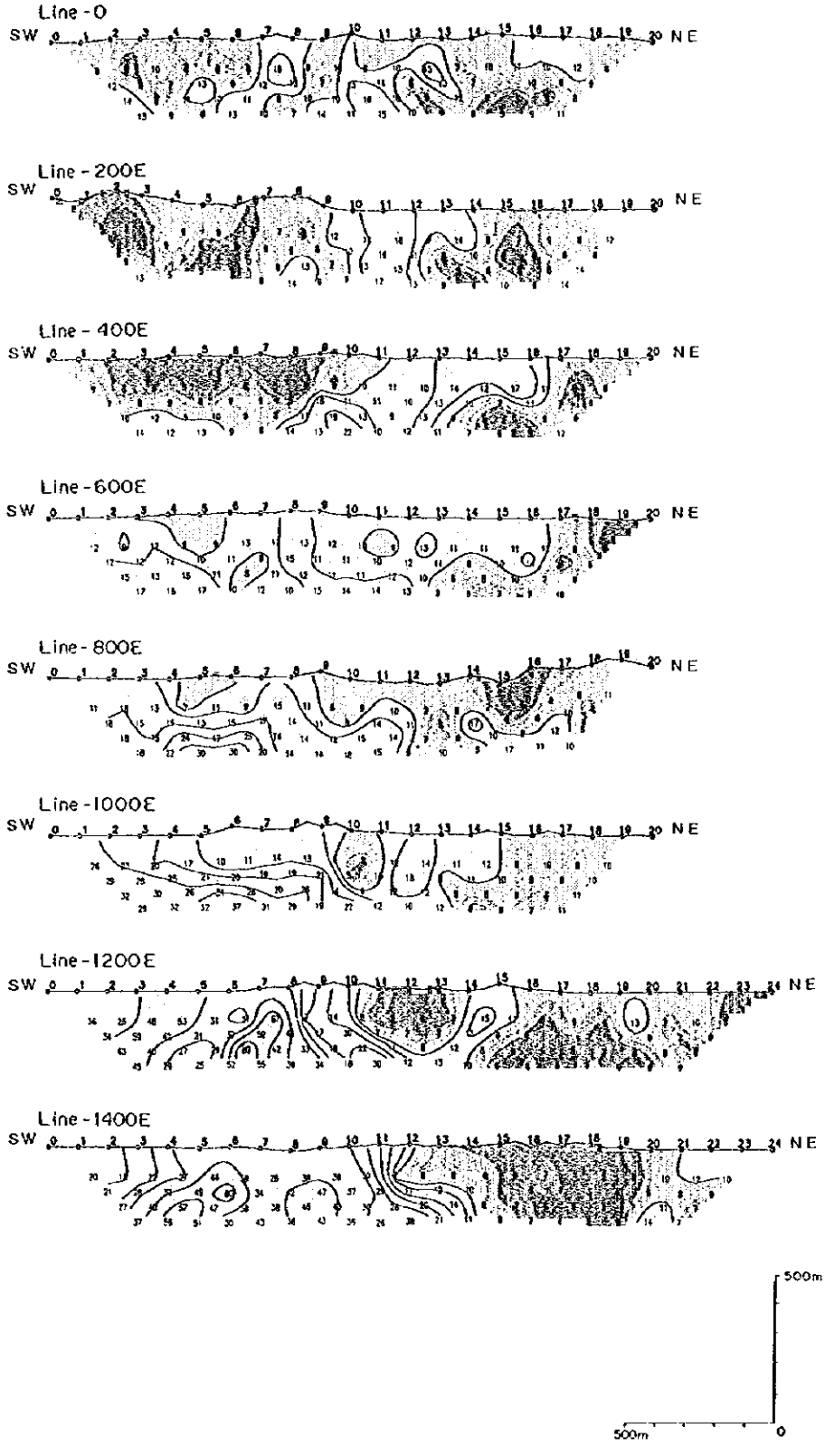

Fig. II-4-16 Metal factor pseudo-sections in Ghuzayn East area

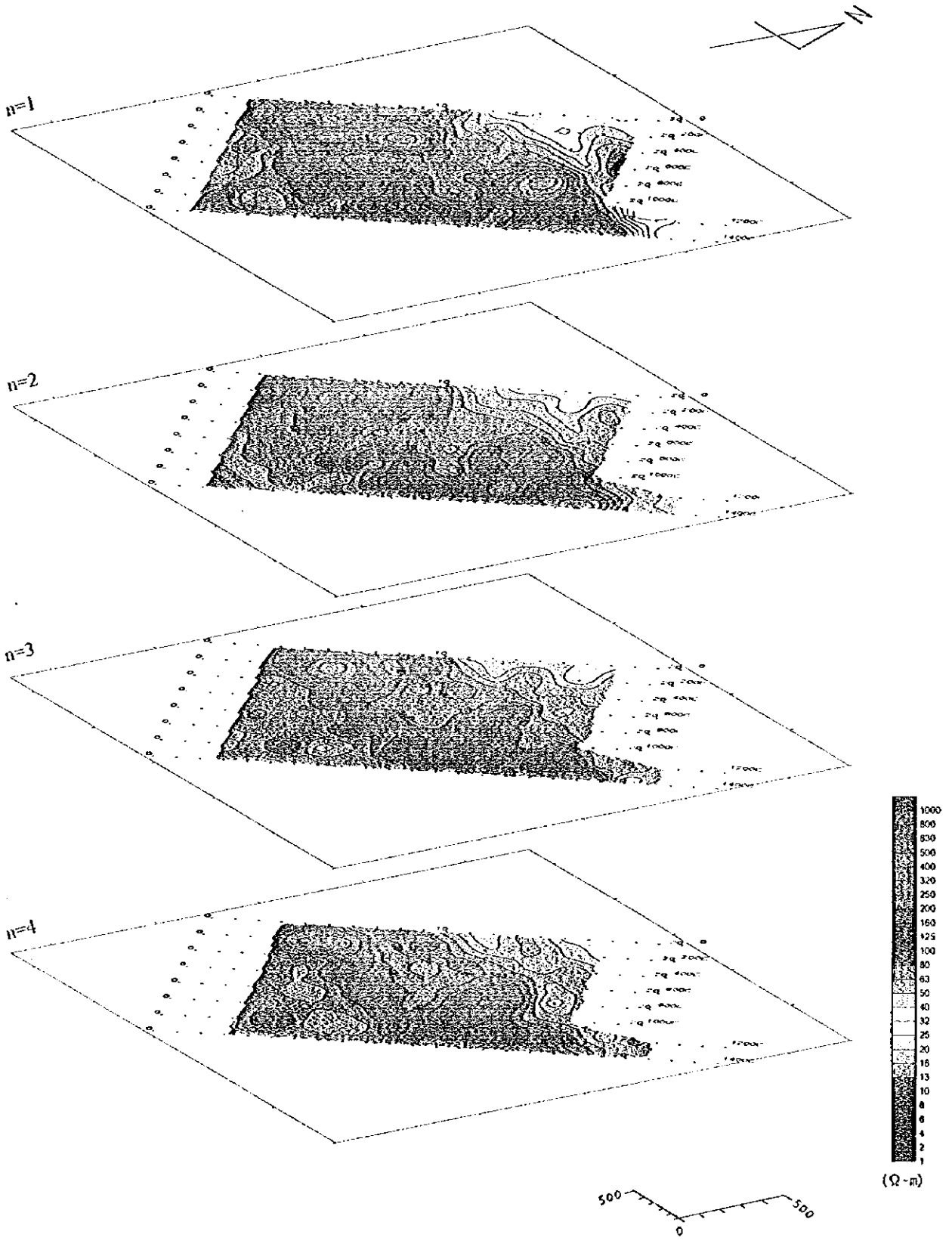

Fig. II-4-17 Apparent resistivity plan map in Ghuzayn East area

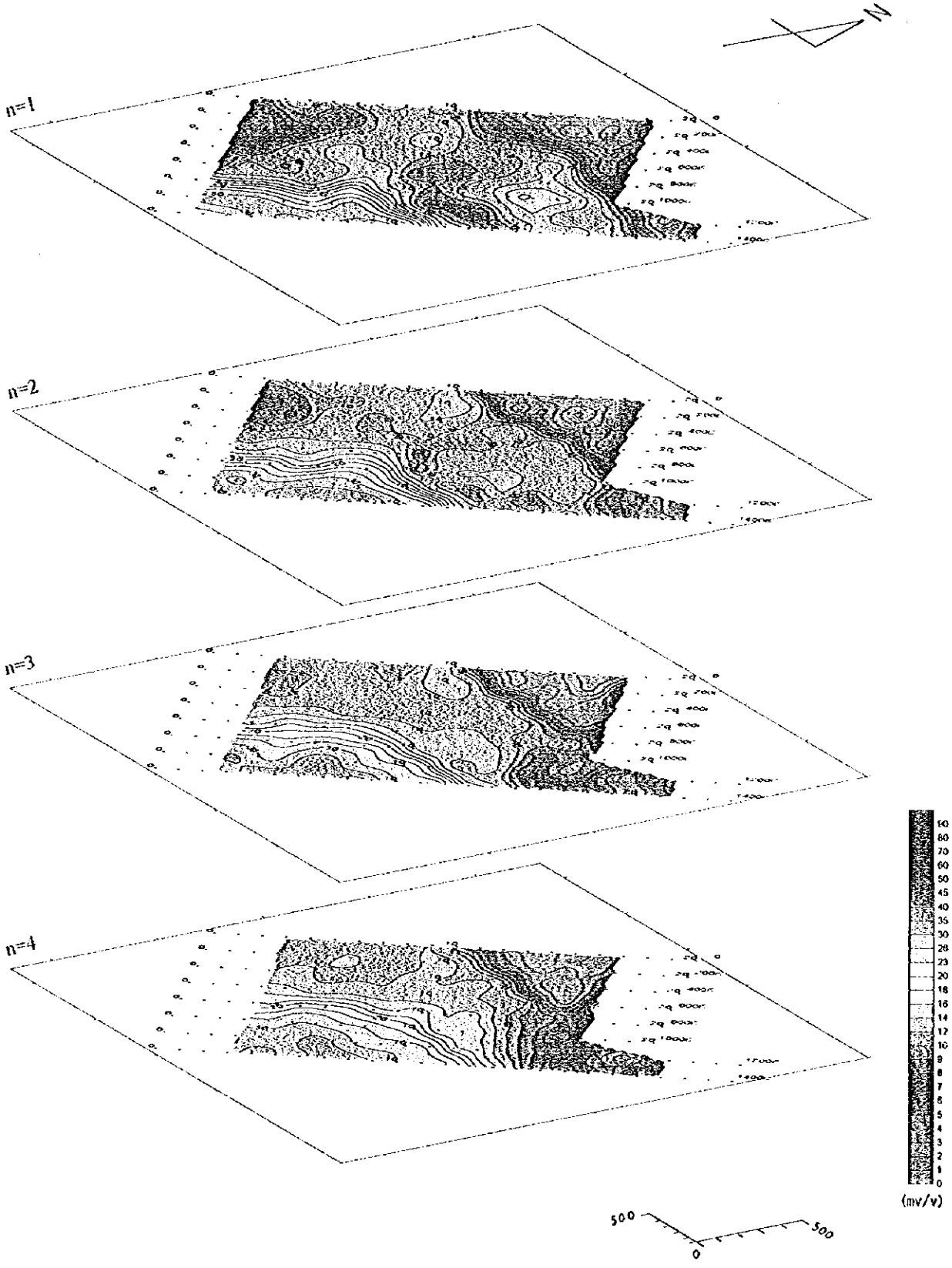

Fig. II-4-18 Chargeability plan map in Ghuzayn East area

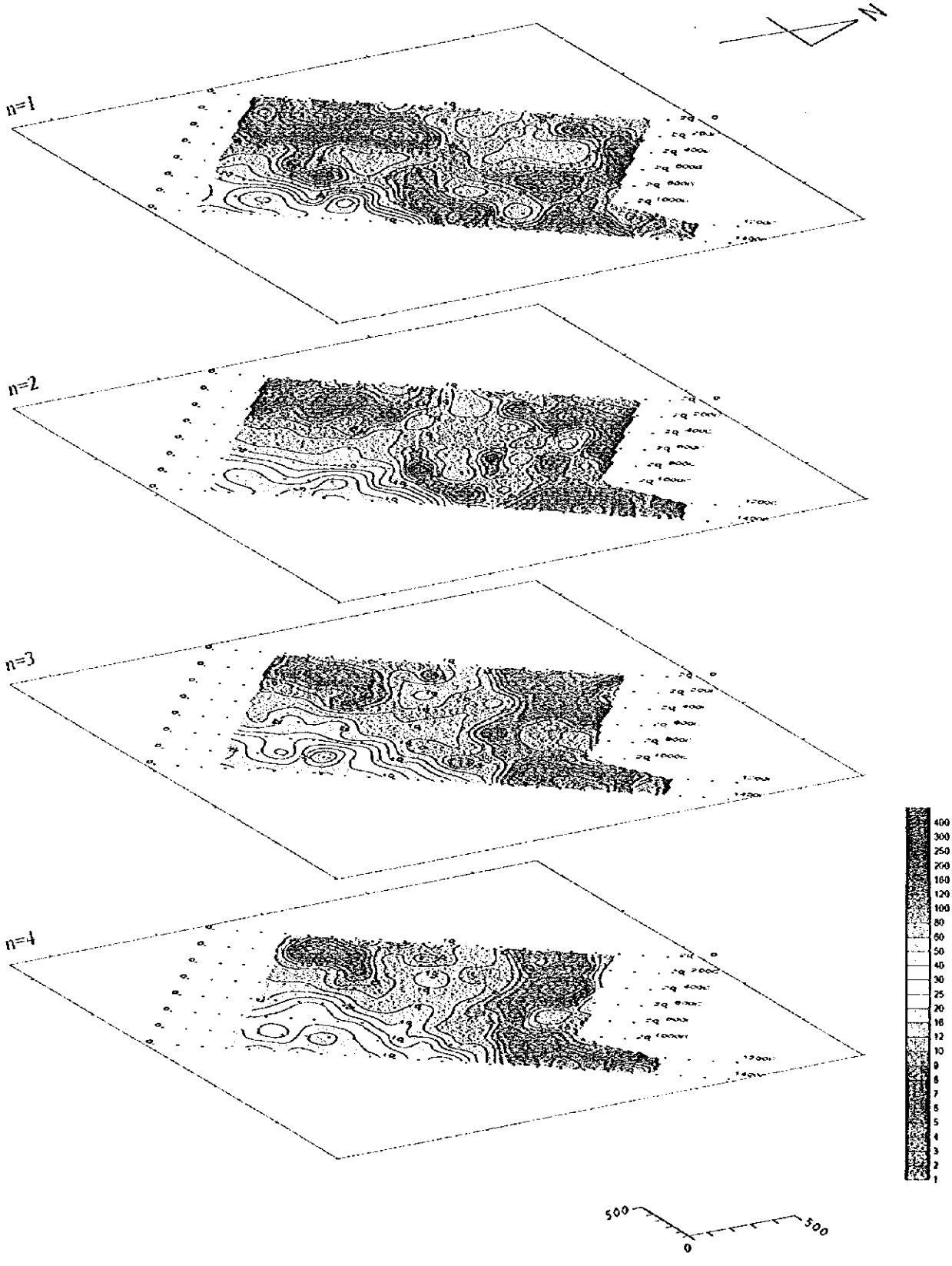

Fig. II -4-19 Metal factor plan map in Ghuzayn East area

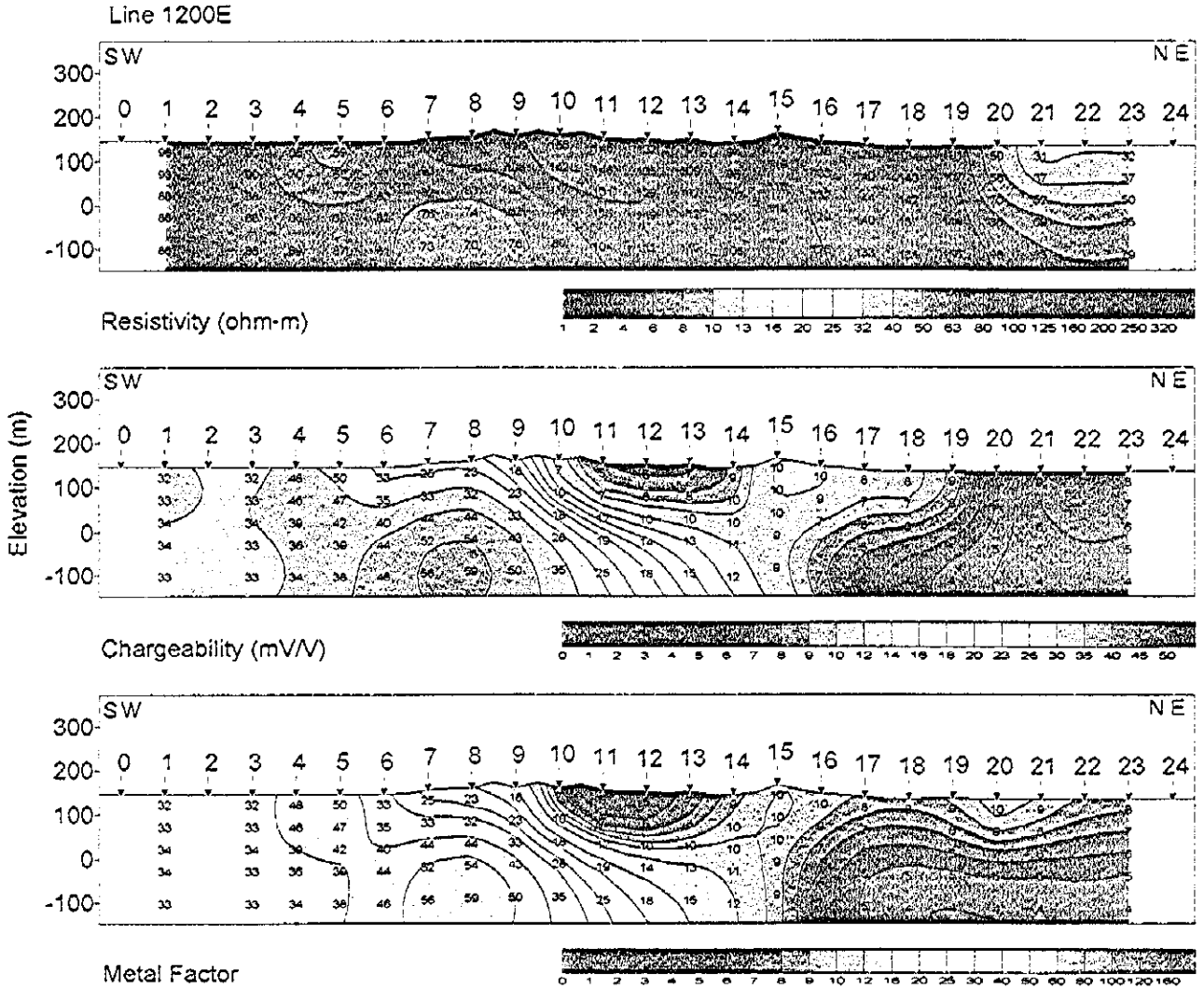

Fig. II-4-20 Results of model simulation in Ghuzayn East area(1)

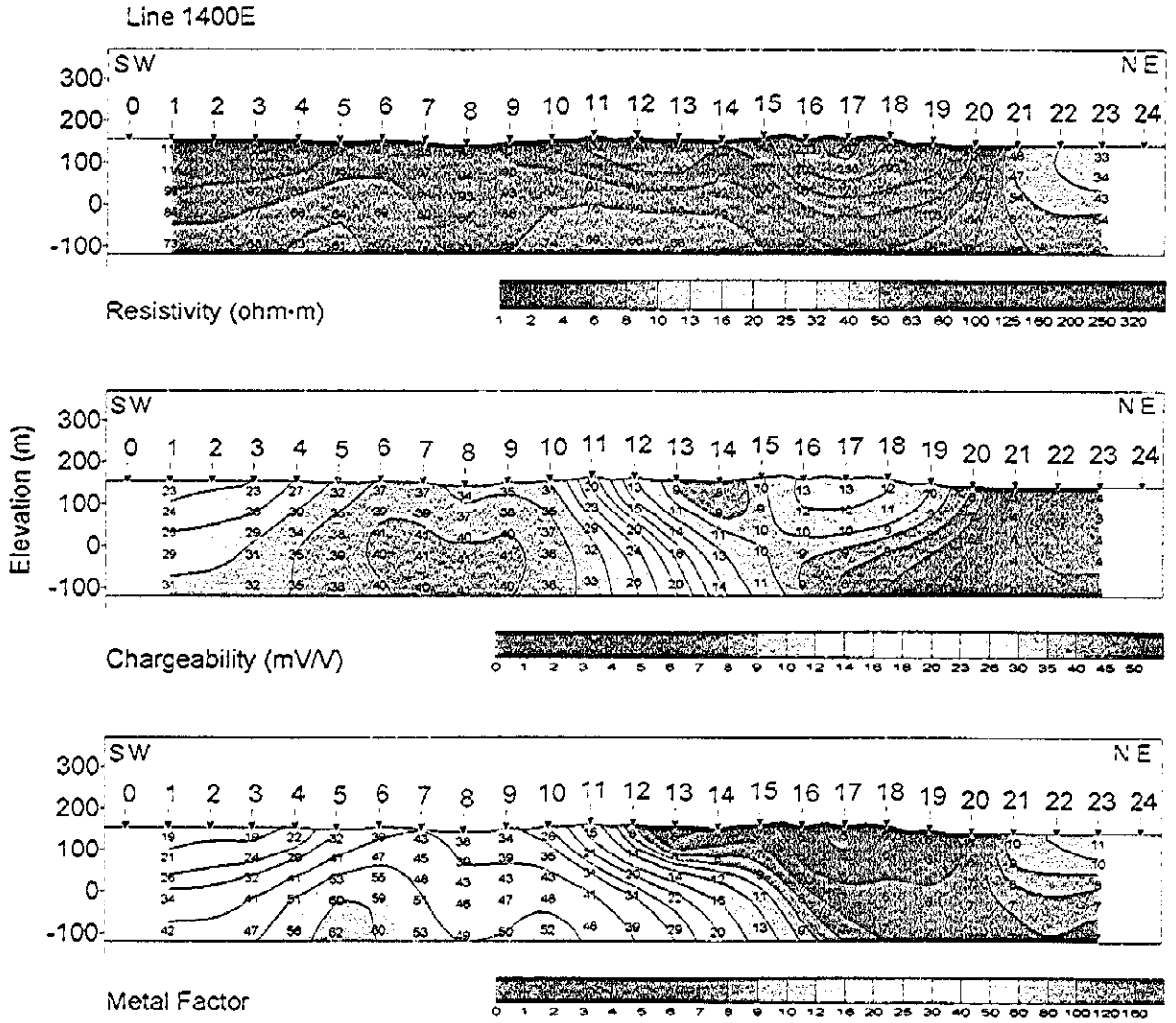

Fig. II -4-21 Results of model simulation in Ghuzayn East area(2)

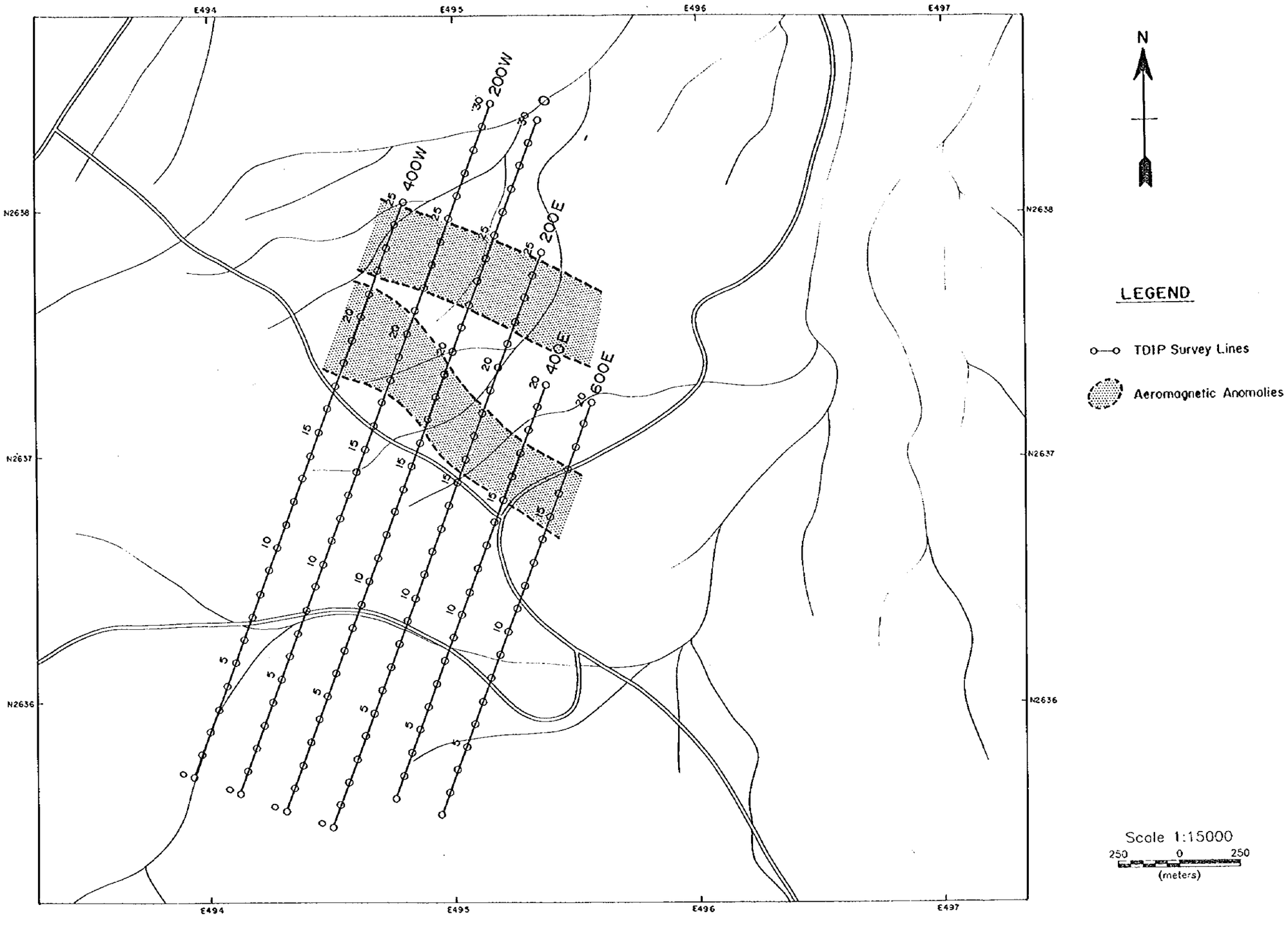

Fig. II-4-22 IP line locations in Ghuzayn West area

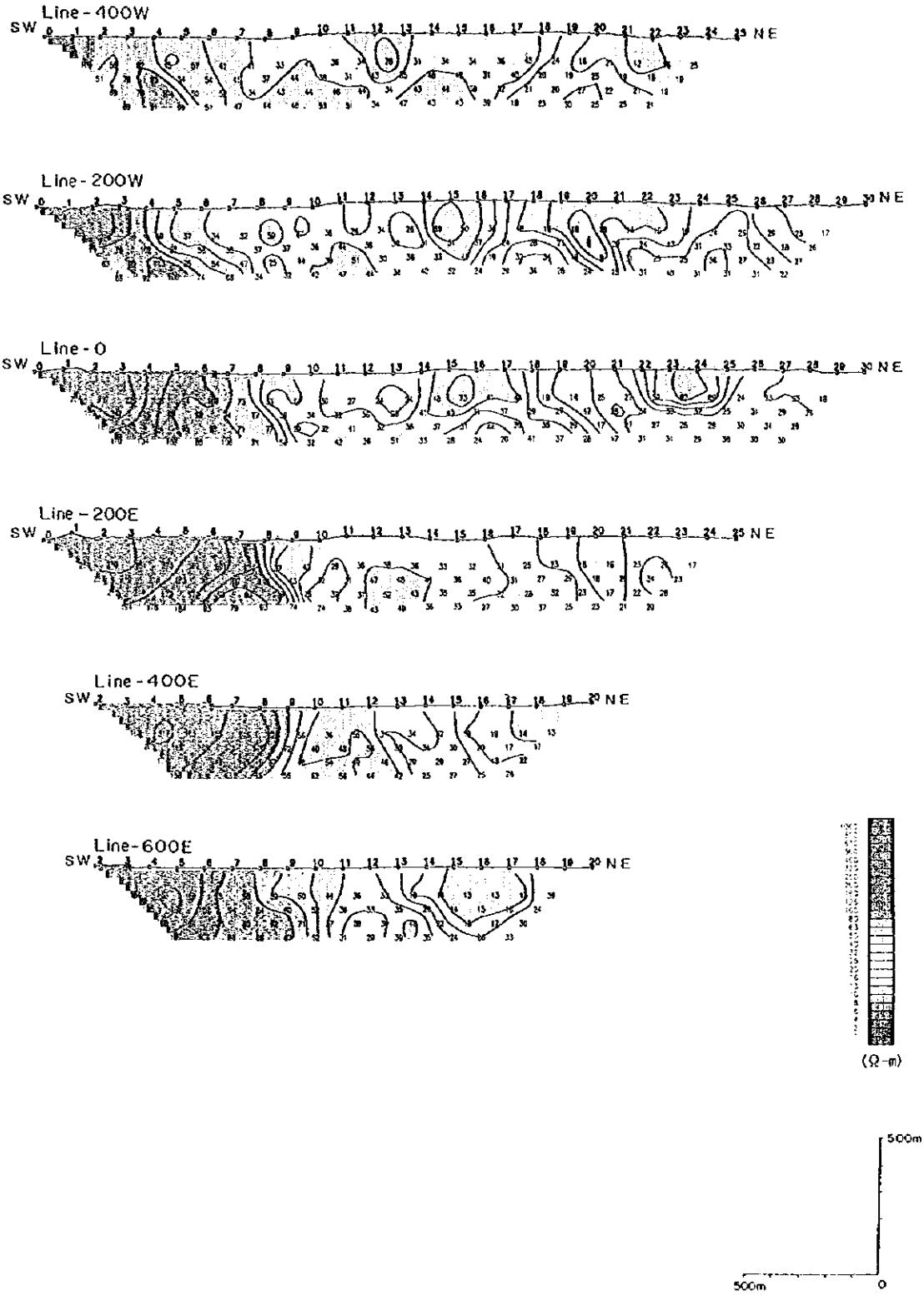

Fig. II -4-23 Apparent resistivity pseudo-sections in Ghuzayn West area

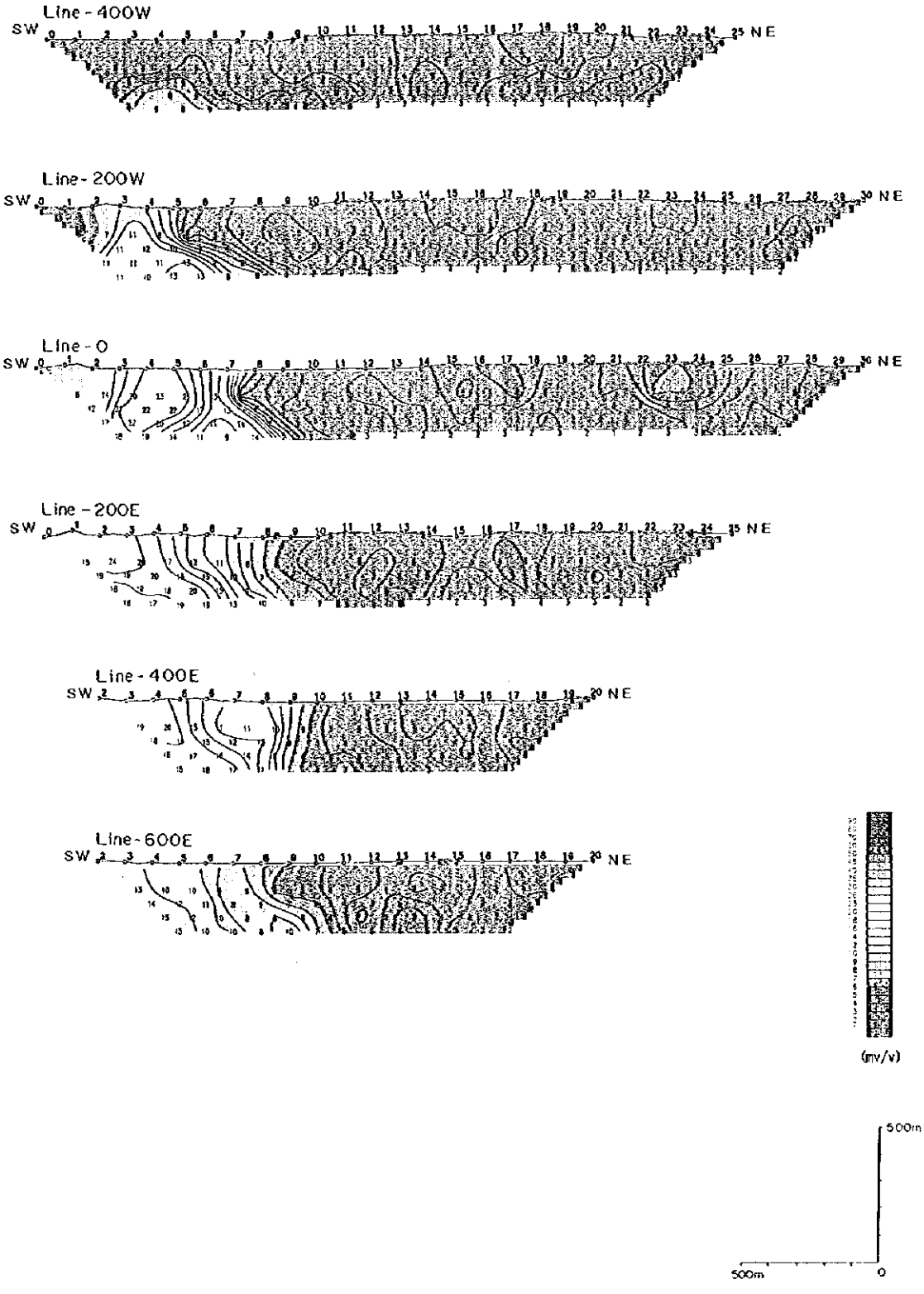

Fig. II -4-24 Chargeability pseudo-sections in Ghuzayn West area

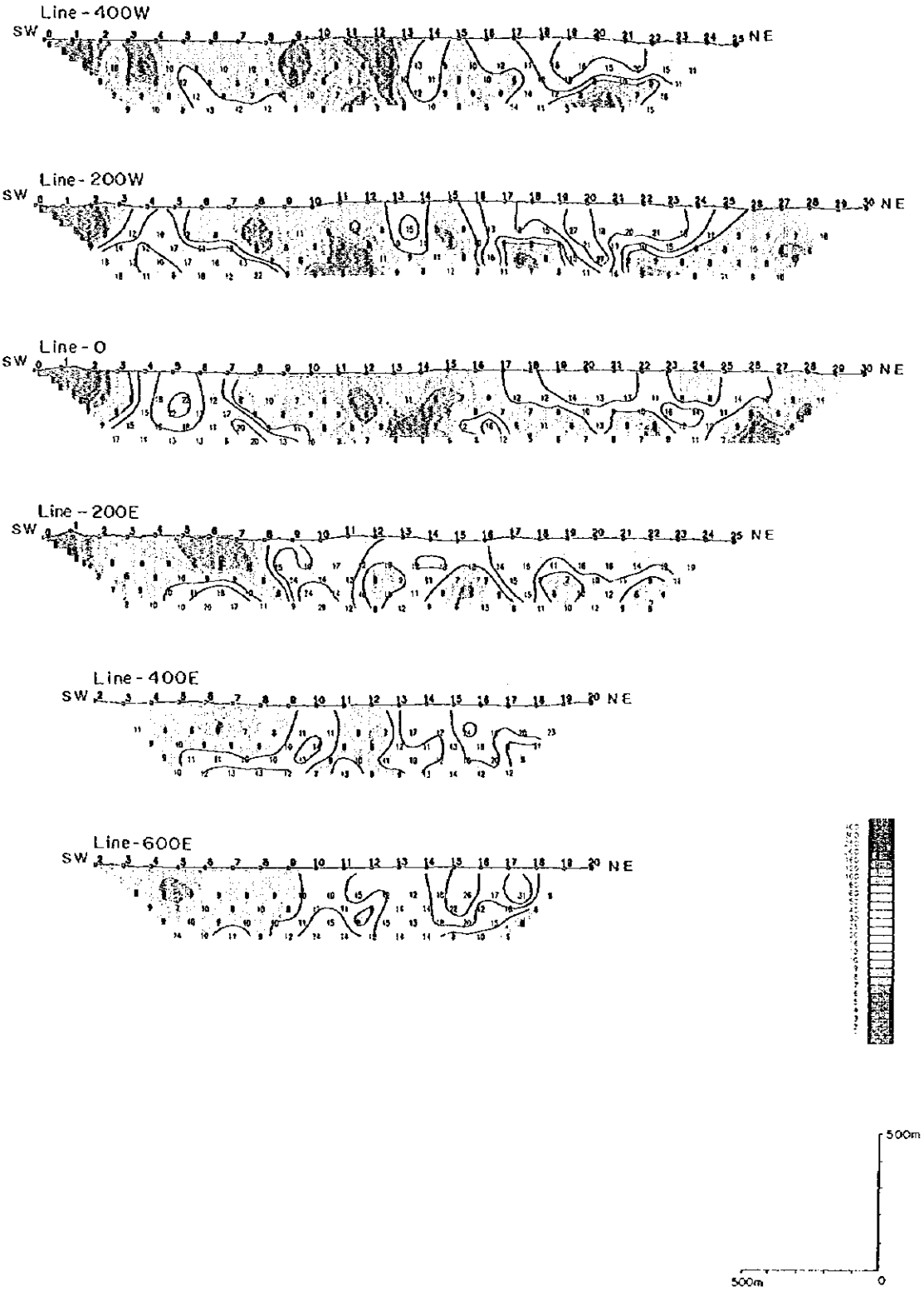

Fig. II -4-25 Metal factor pseudo-sections in Ghuzayn West area

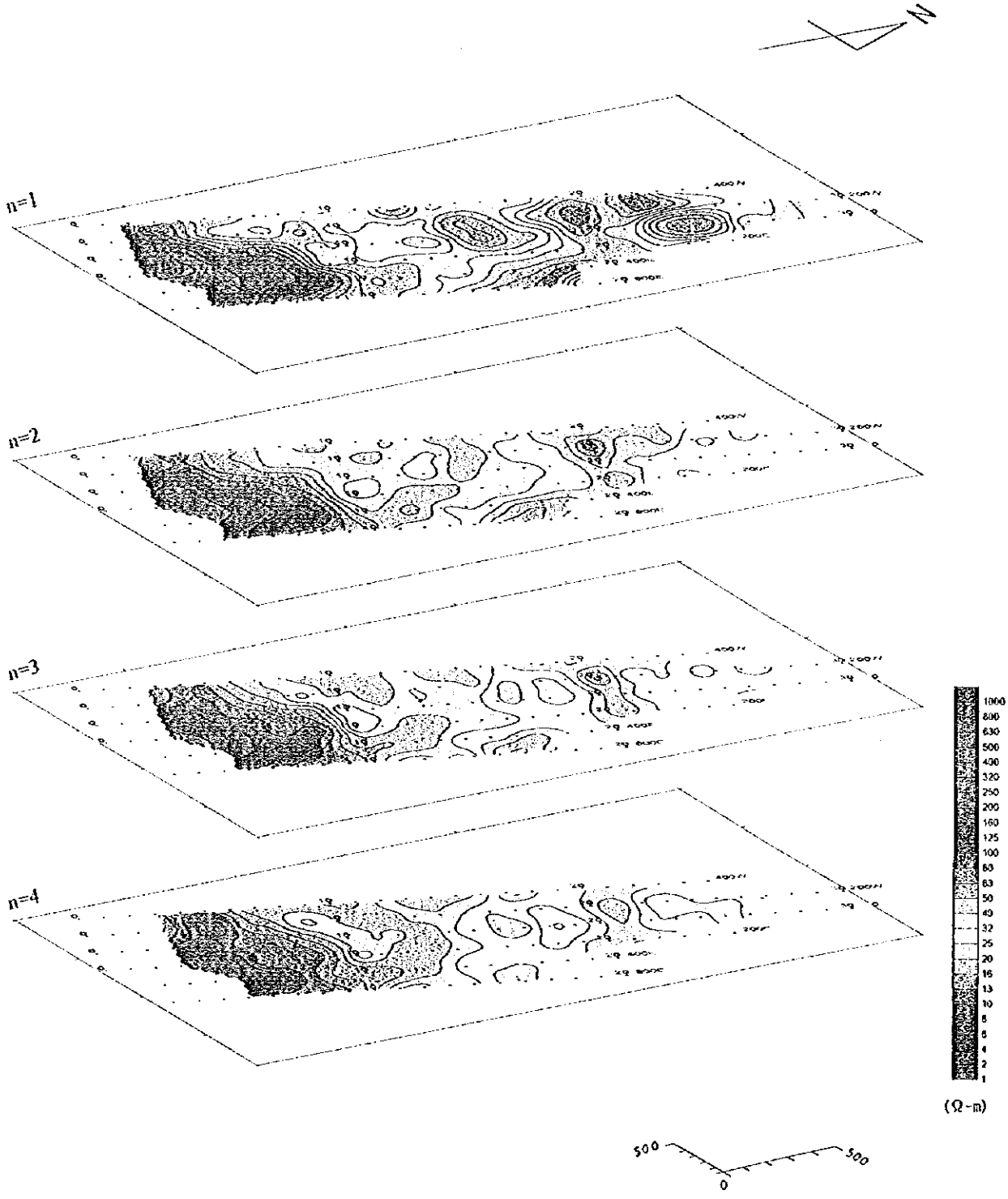

Fig. II -4-26 Apparent resistivity plan map in Ghuzayn West area

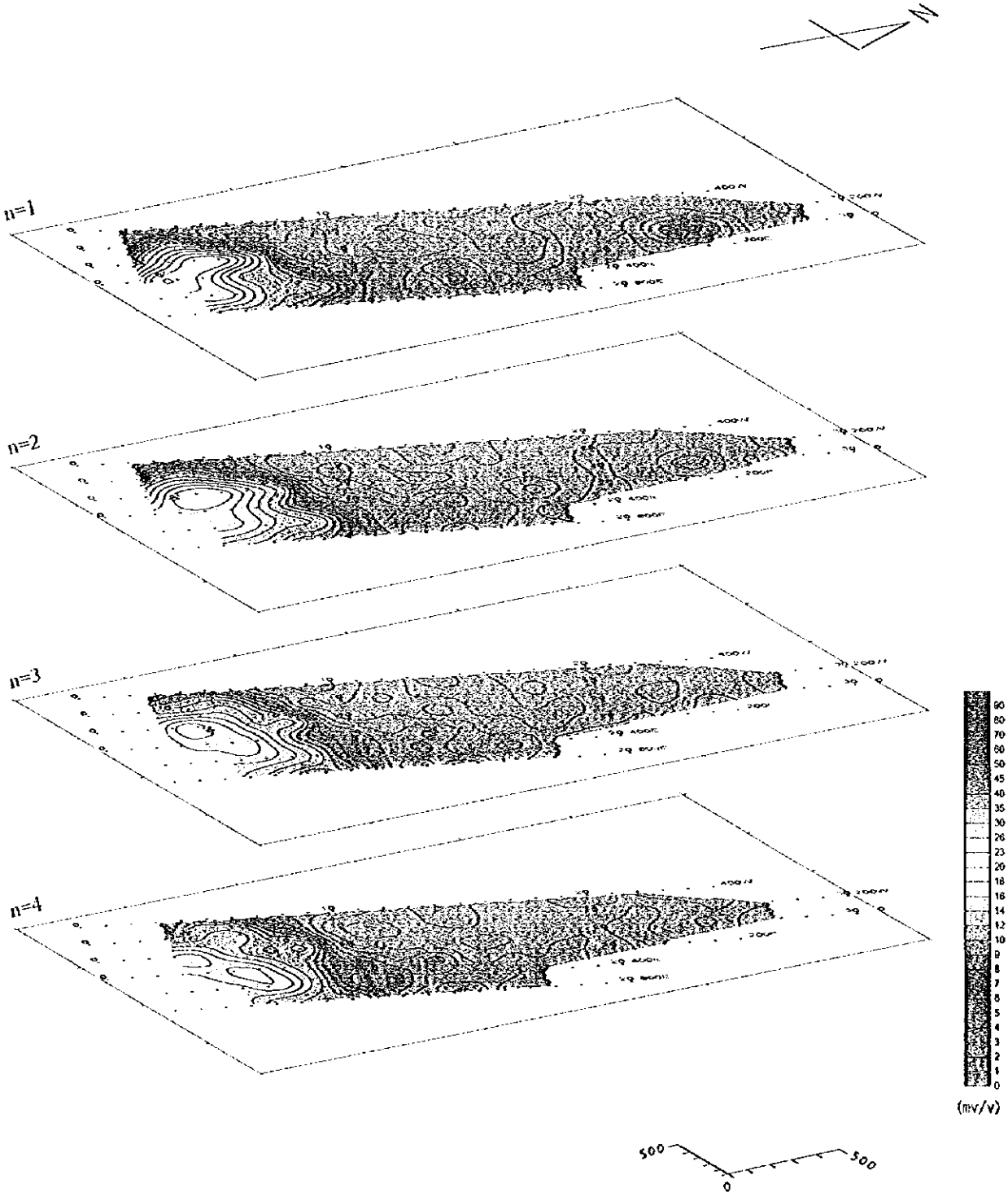

Fig. II -4-27 Chargeability plan map in Ghuzayn West area

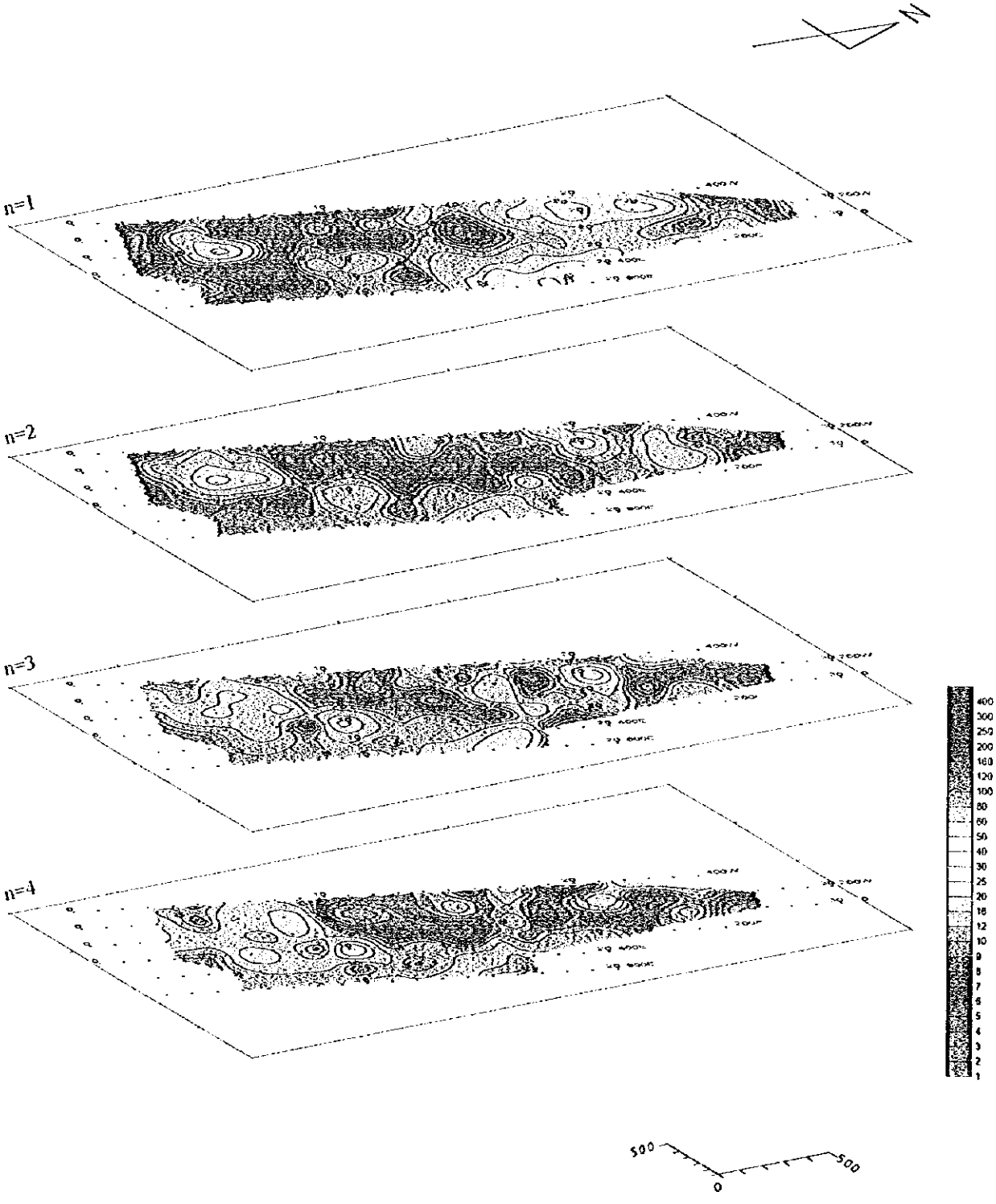

Fig. II -4-28 Metal factor plan map in Ghuzayn West area

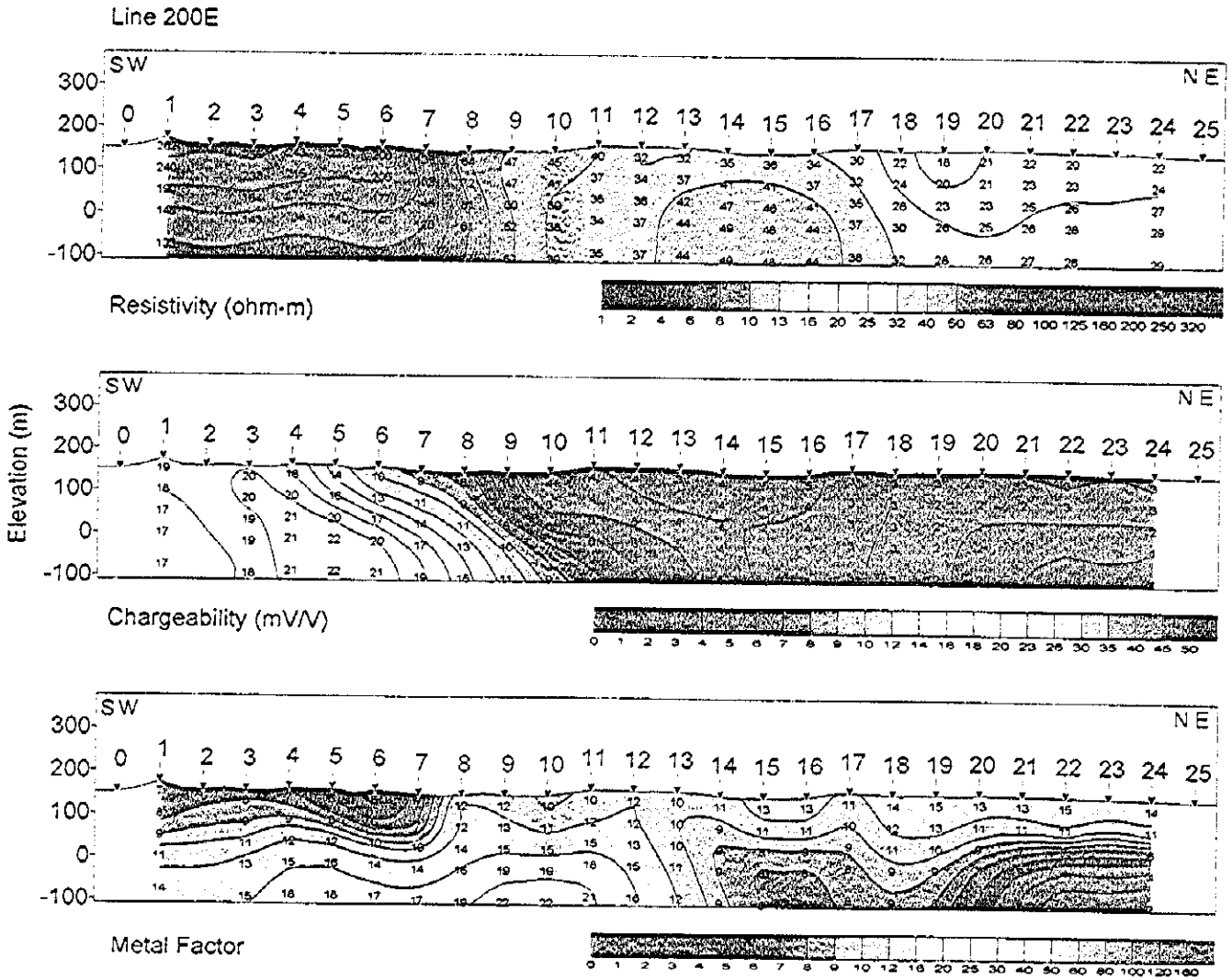

Fig. II -4-29 Results of model simulation in Ghuzayn West area(1)

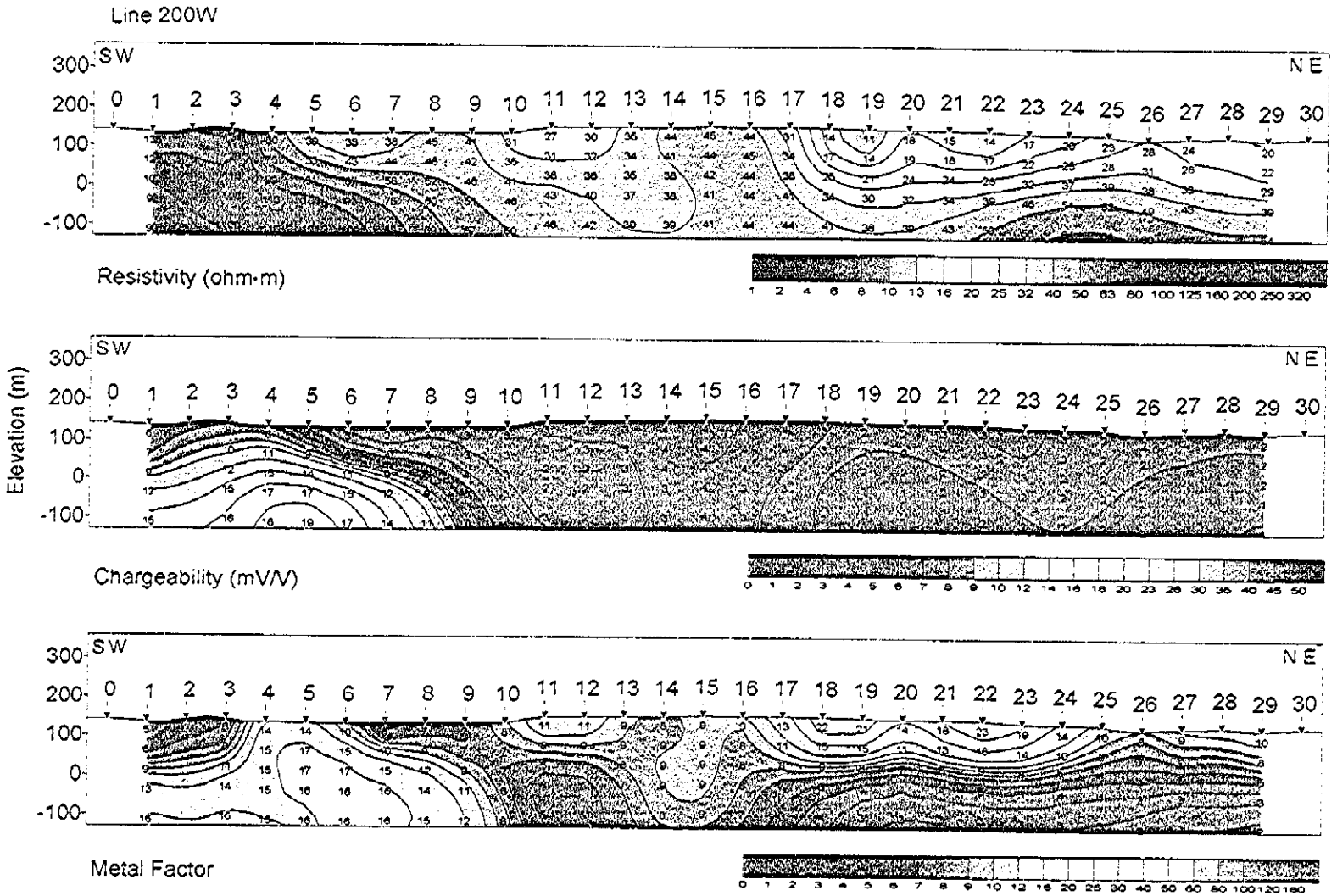

Fig. II-4-30 Results of model simulation in Ghuzayn West area(2)

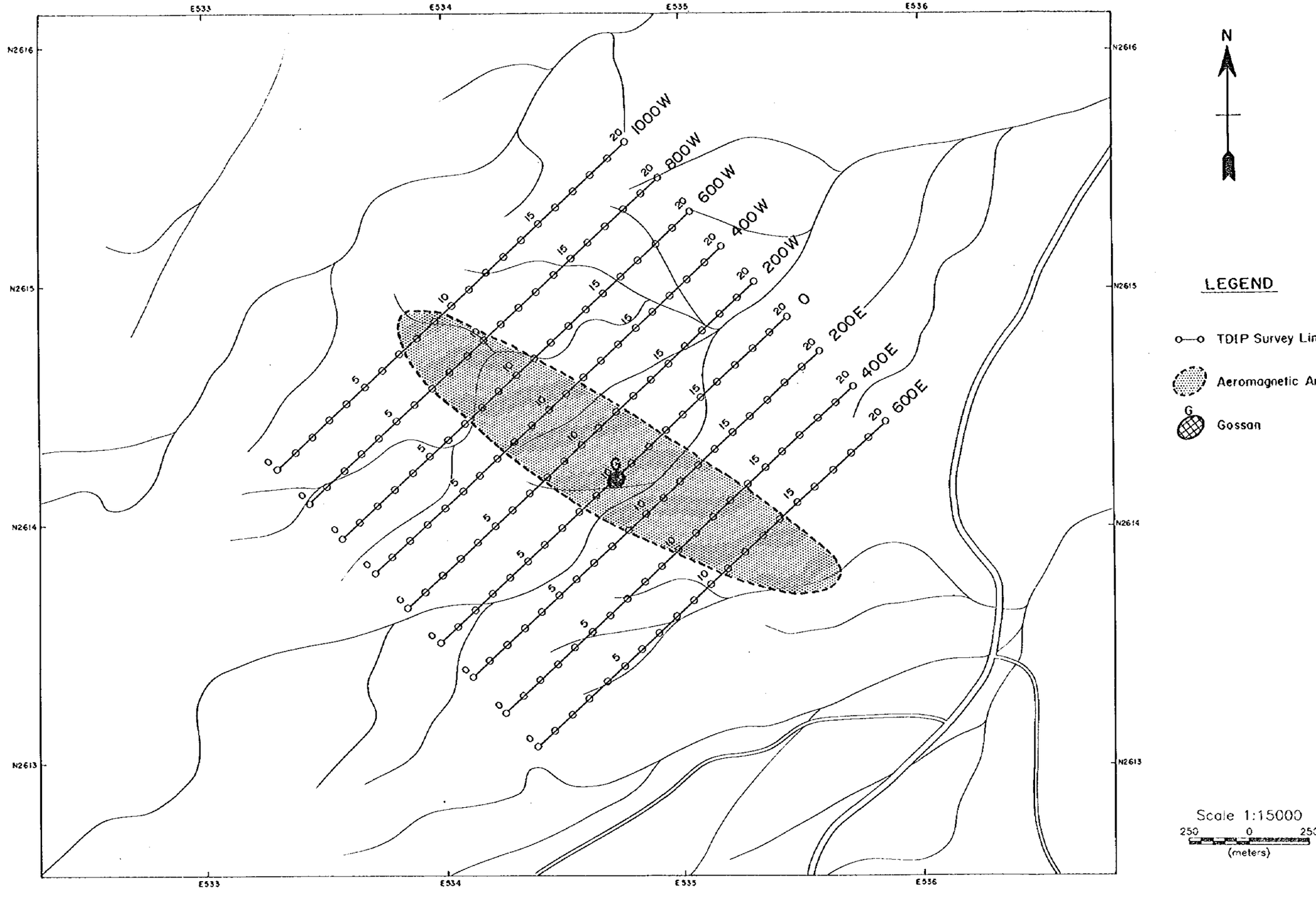

Fig. II-4-31 IP line locations in Daris 3A5 area

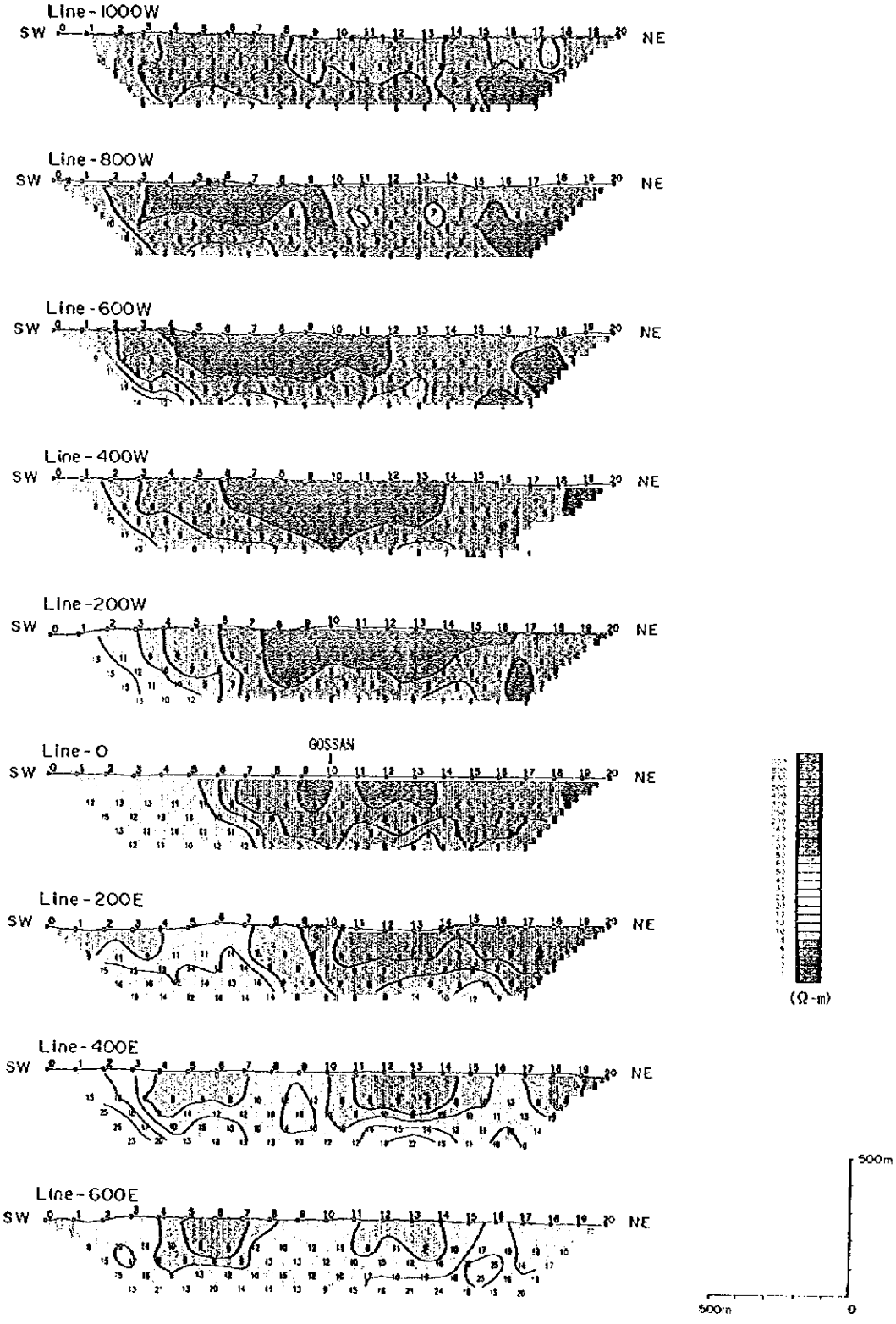

Fig. II-4-32 Apparent resistivity pseudo-sections in Daris 3A5 area

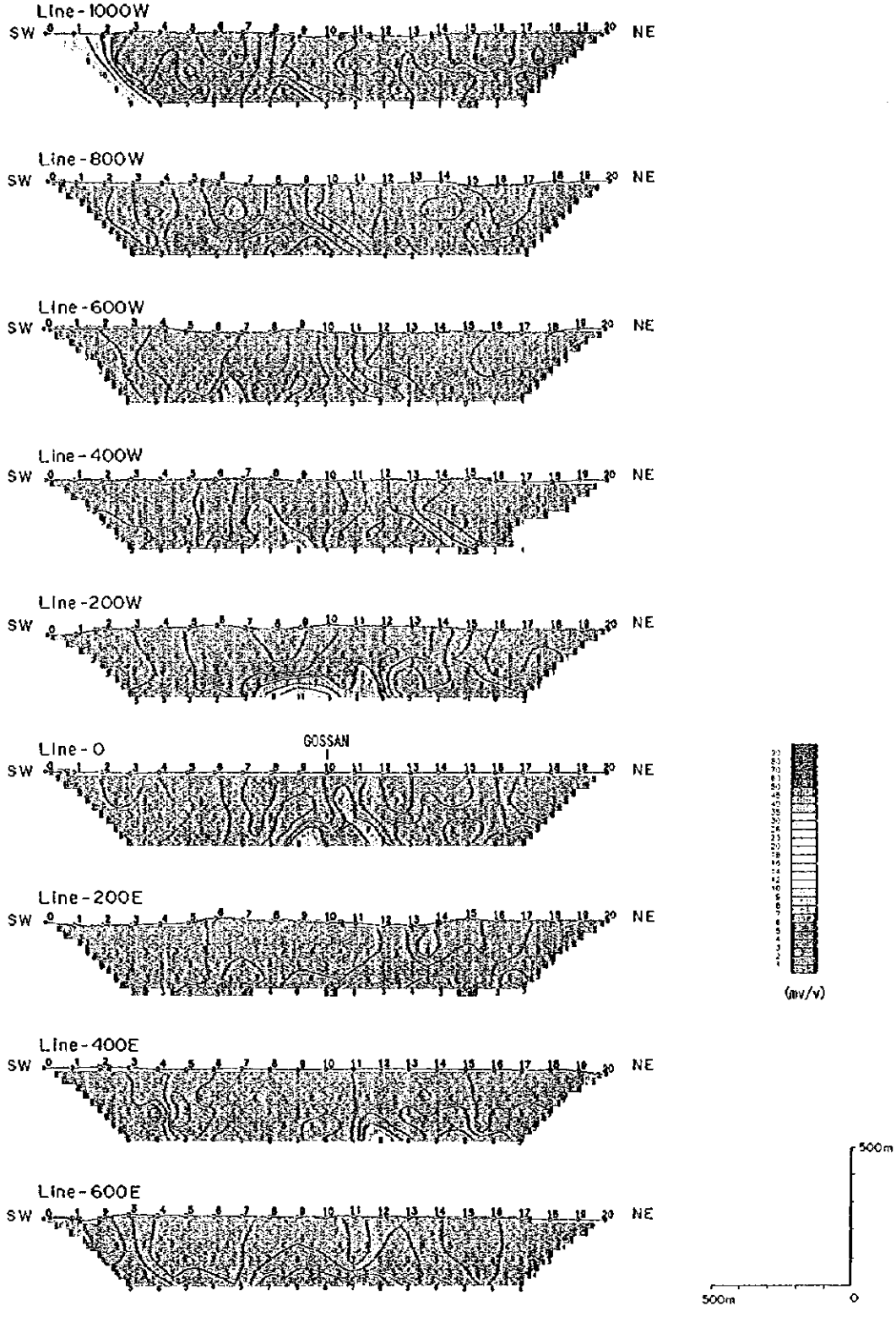

Fig. II-4-33 Chargeability pseudo-sections in Daris 3AS area

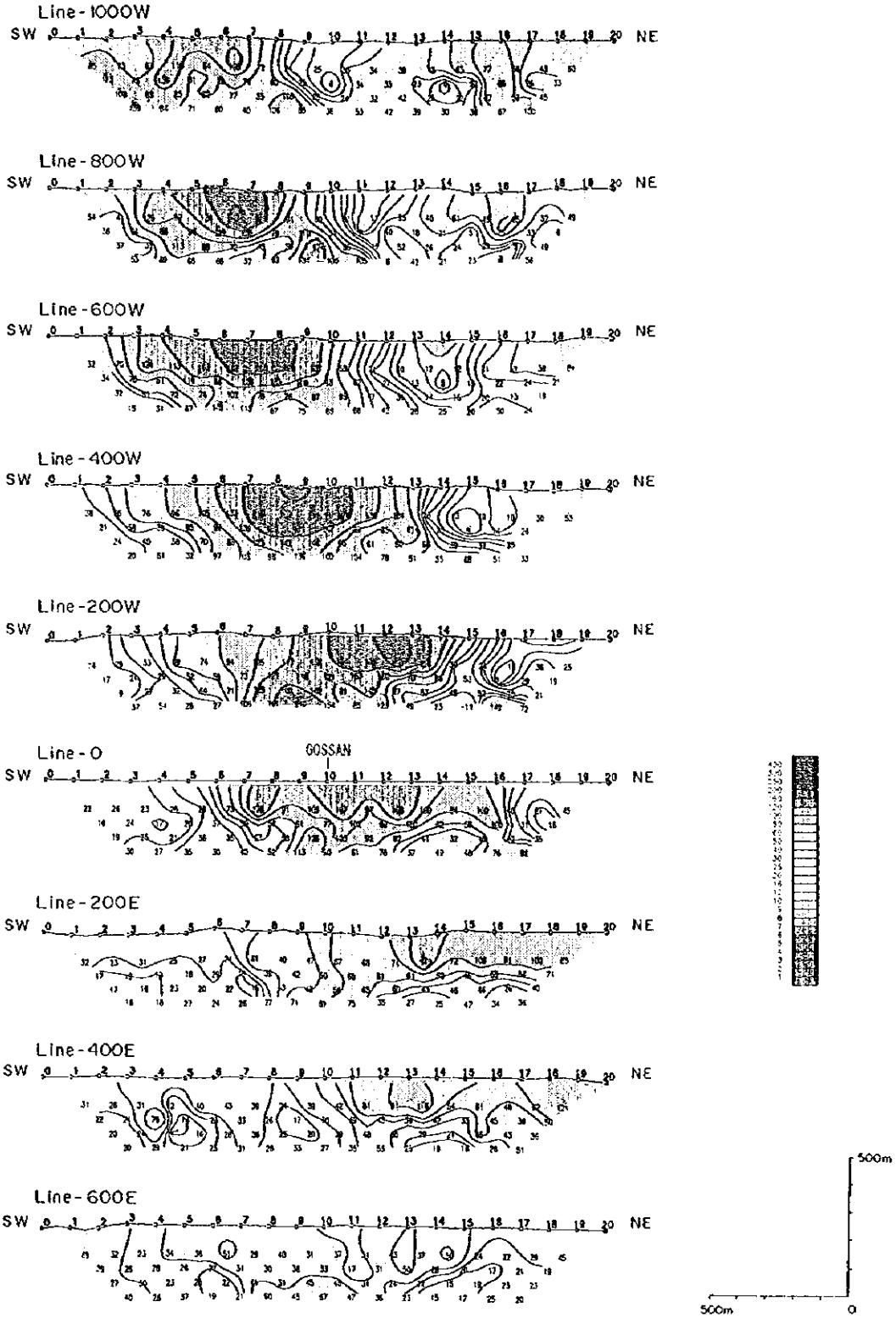

Fig. II-4-34 Metal factor pseudo-sections in Daris 3A5 area

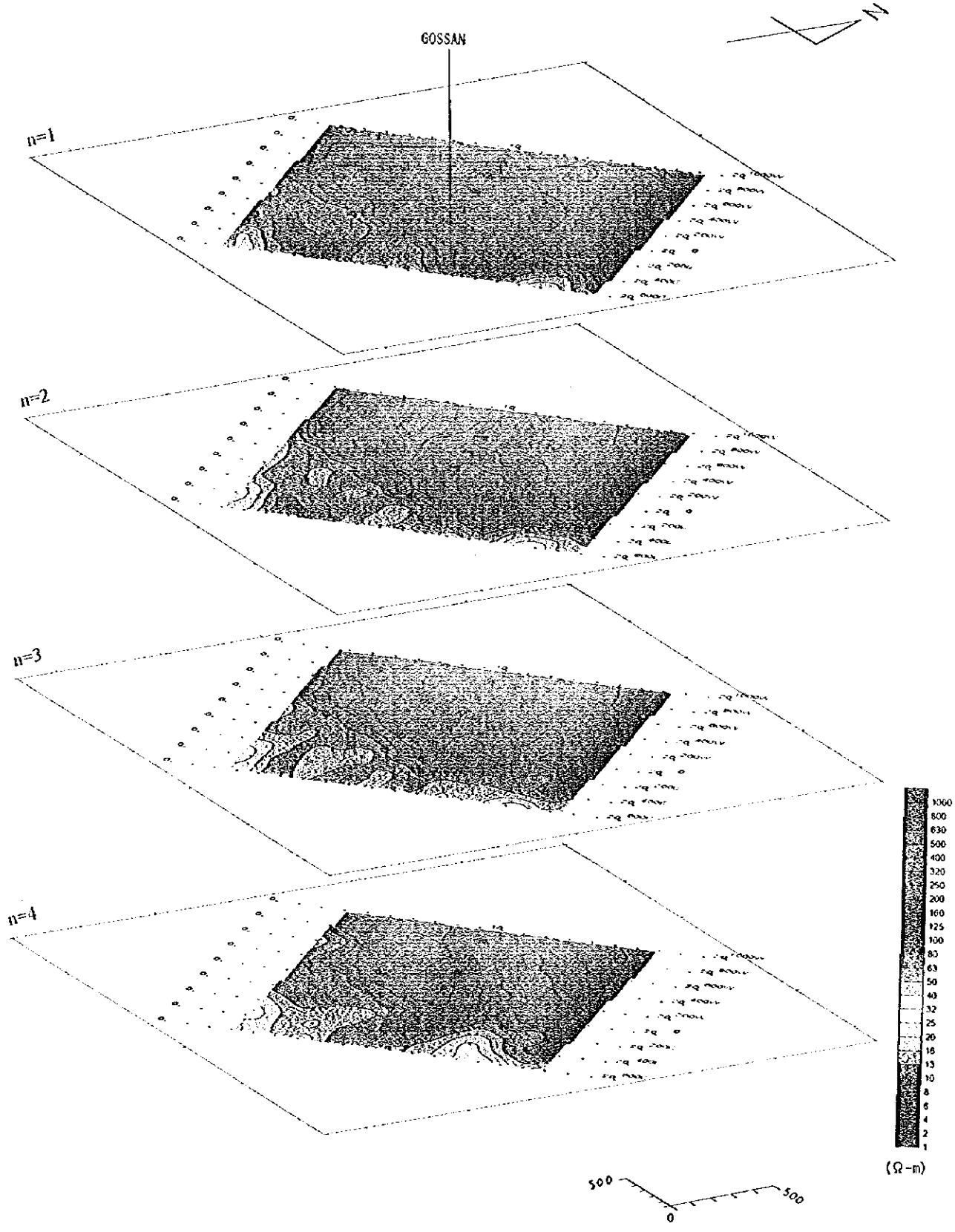

Fig. II-4-35 Apparent resistivity plan map in Daris 3A5 area

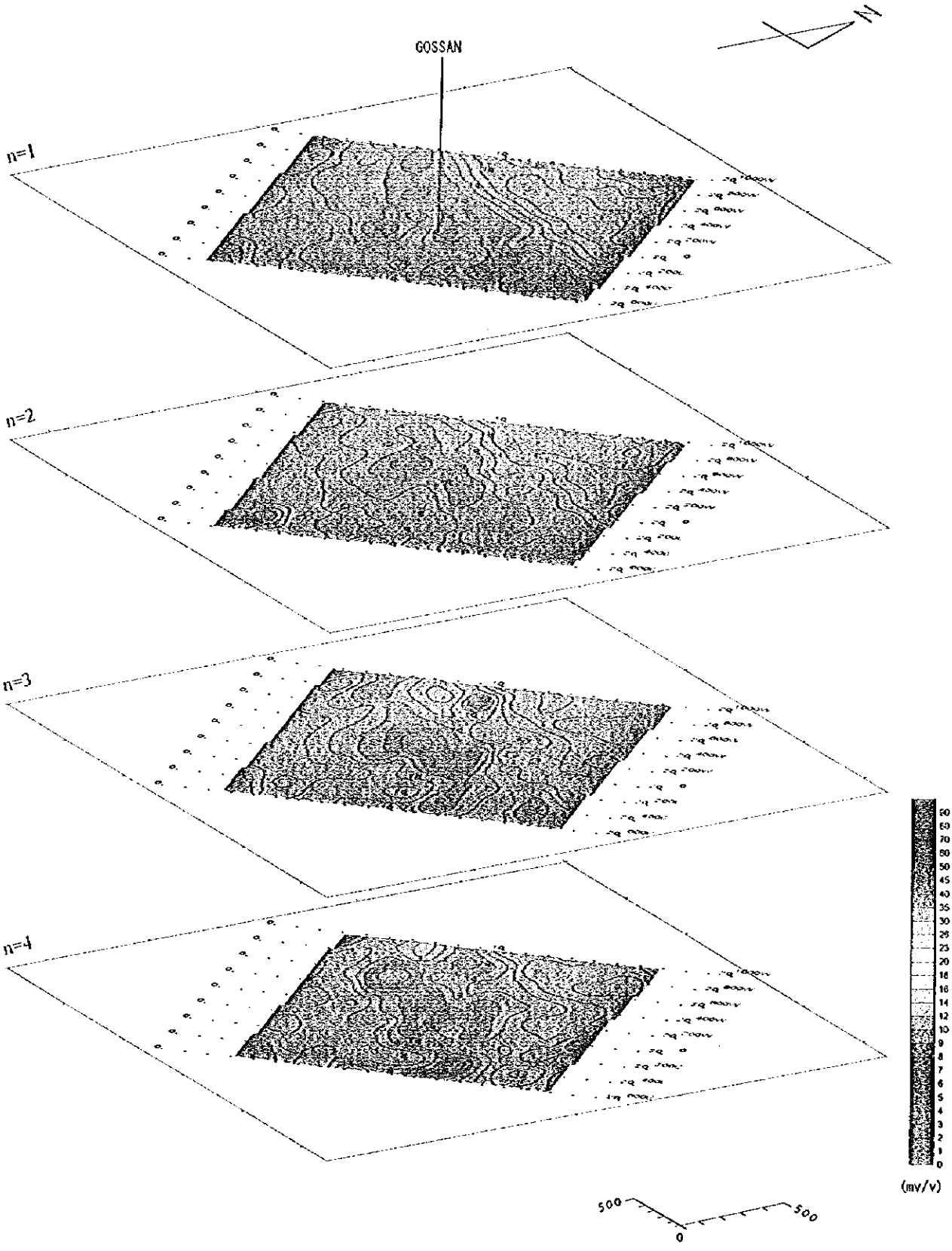

Fig. II -4-36 Chargeability plan map in Daris 3A5 area

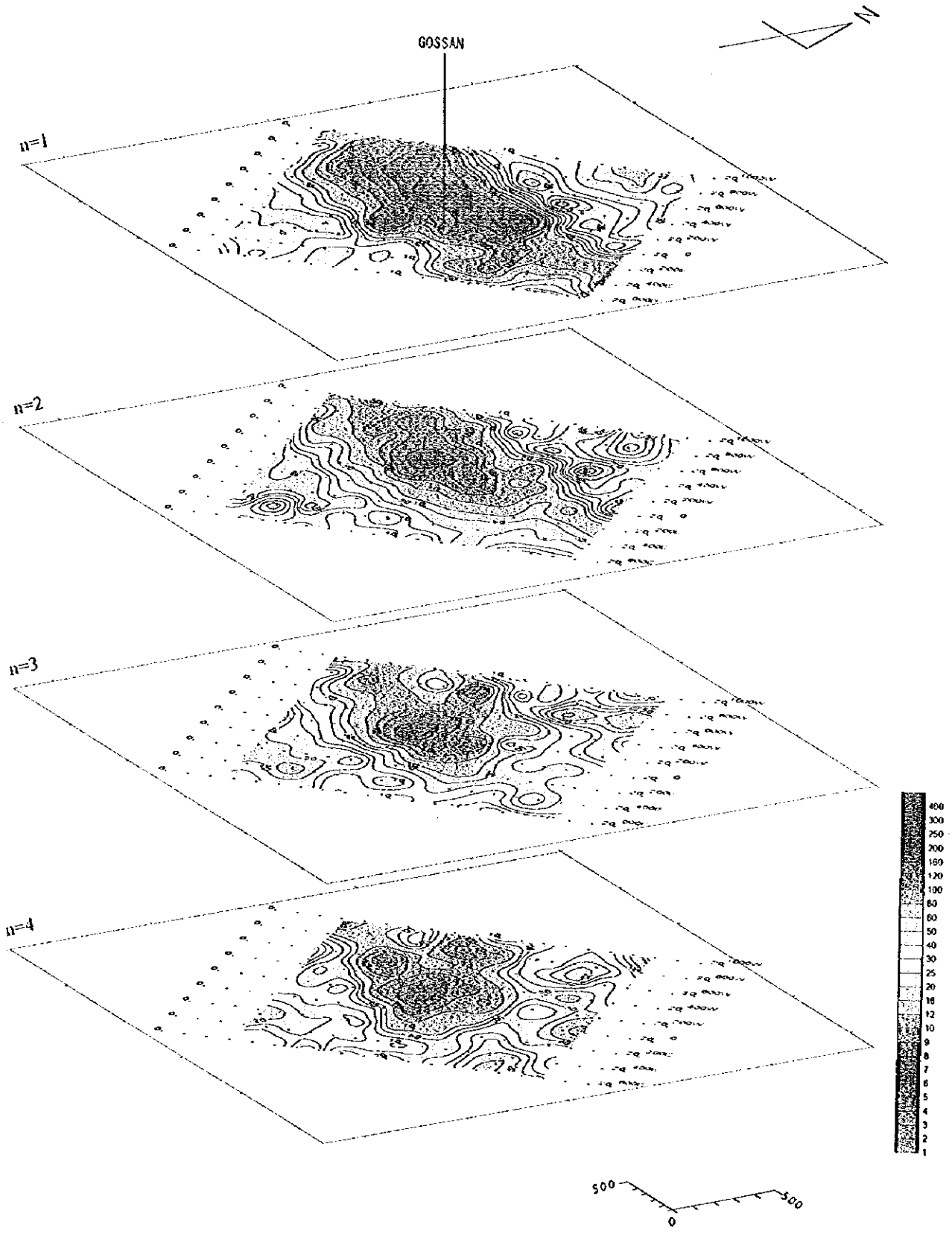

Fig. II -4-37 Metal factor plan map in Daris 3A5 area

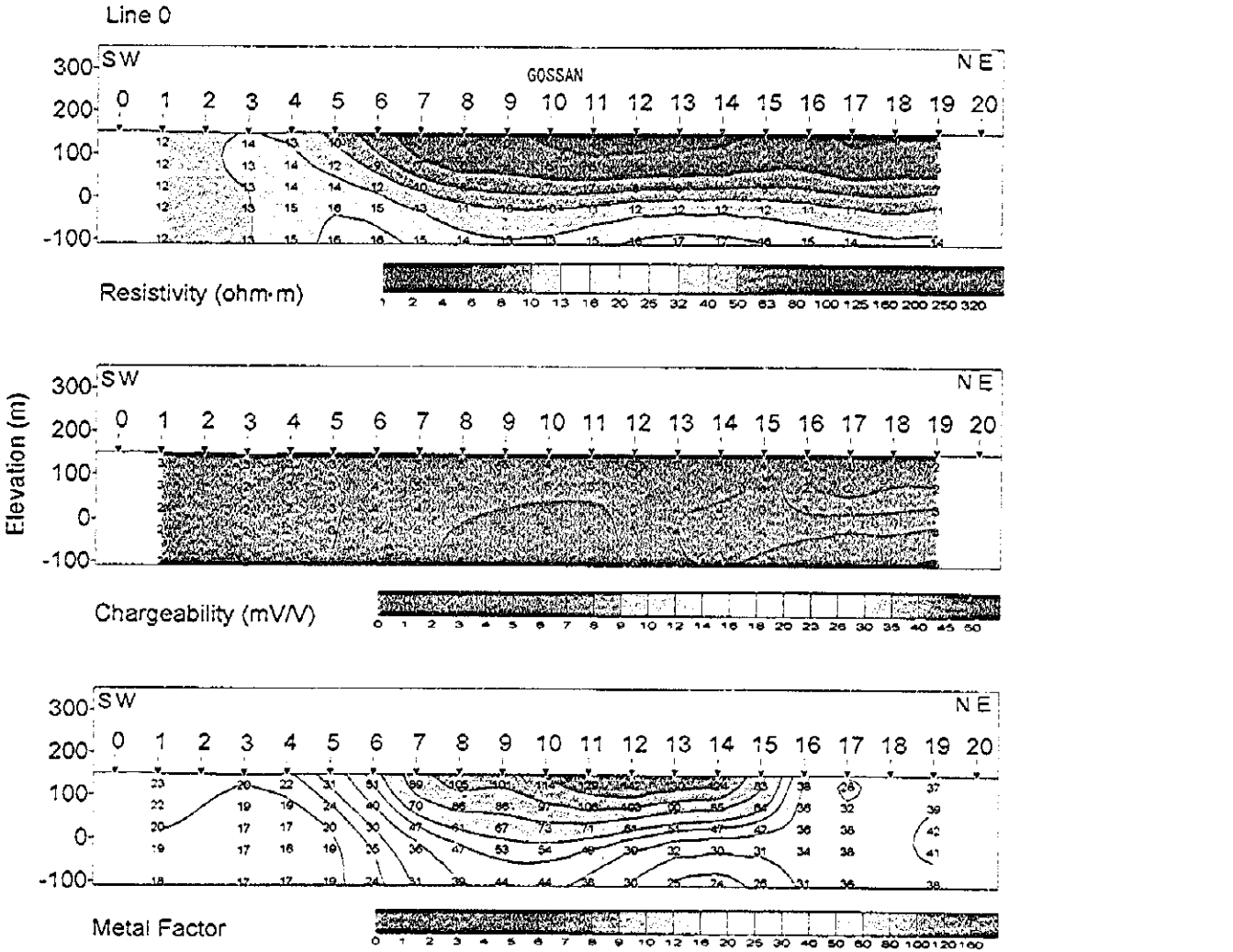

Fig. II-4-38 Results of model simulation in Daris 3A5 area(1)

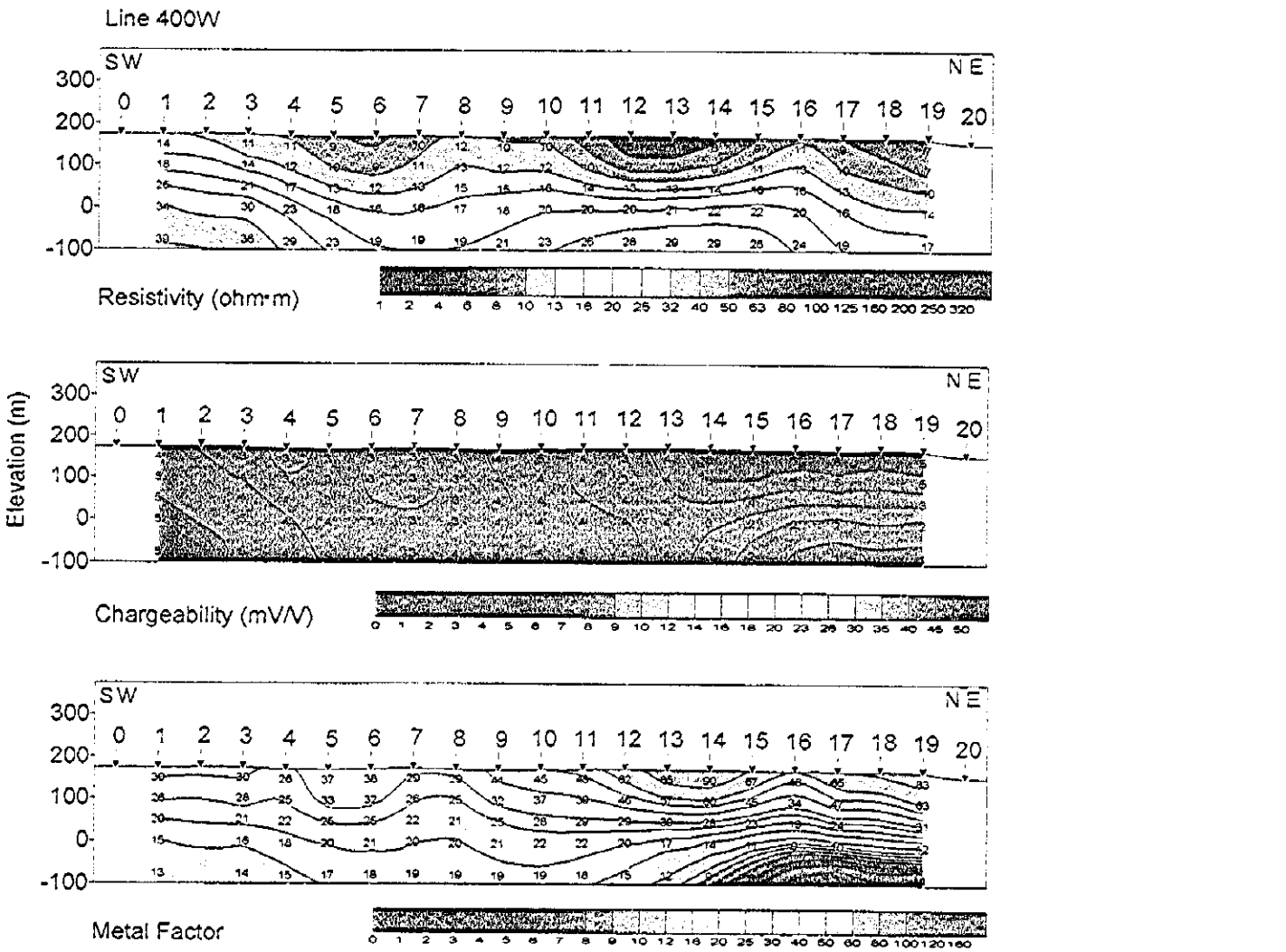

Fig. II -4-39 Results of model simulation in Daris 3A5 area(2)

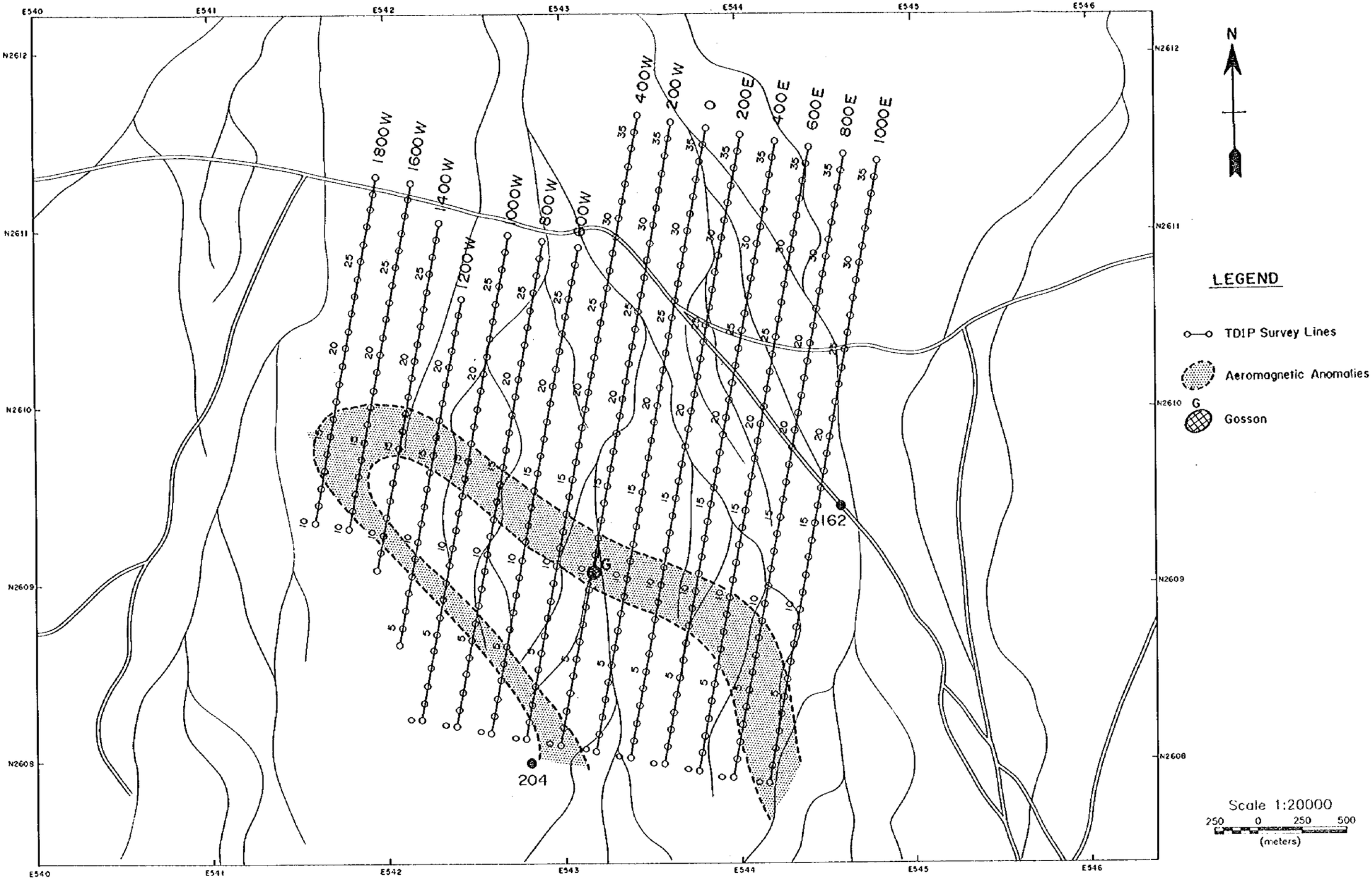

Fig. II-4-40 IP line locations in Daris area

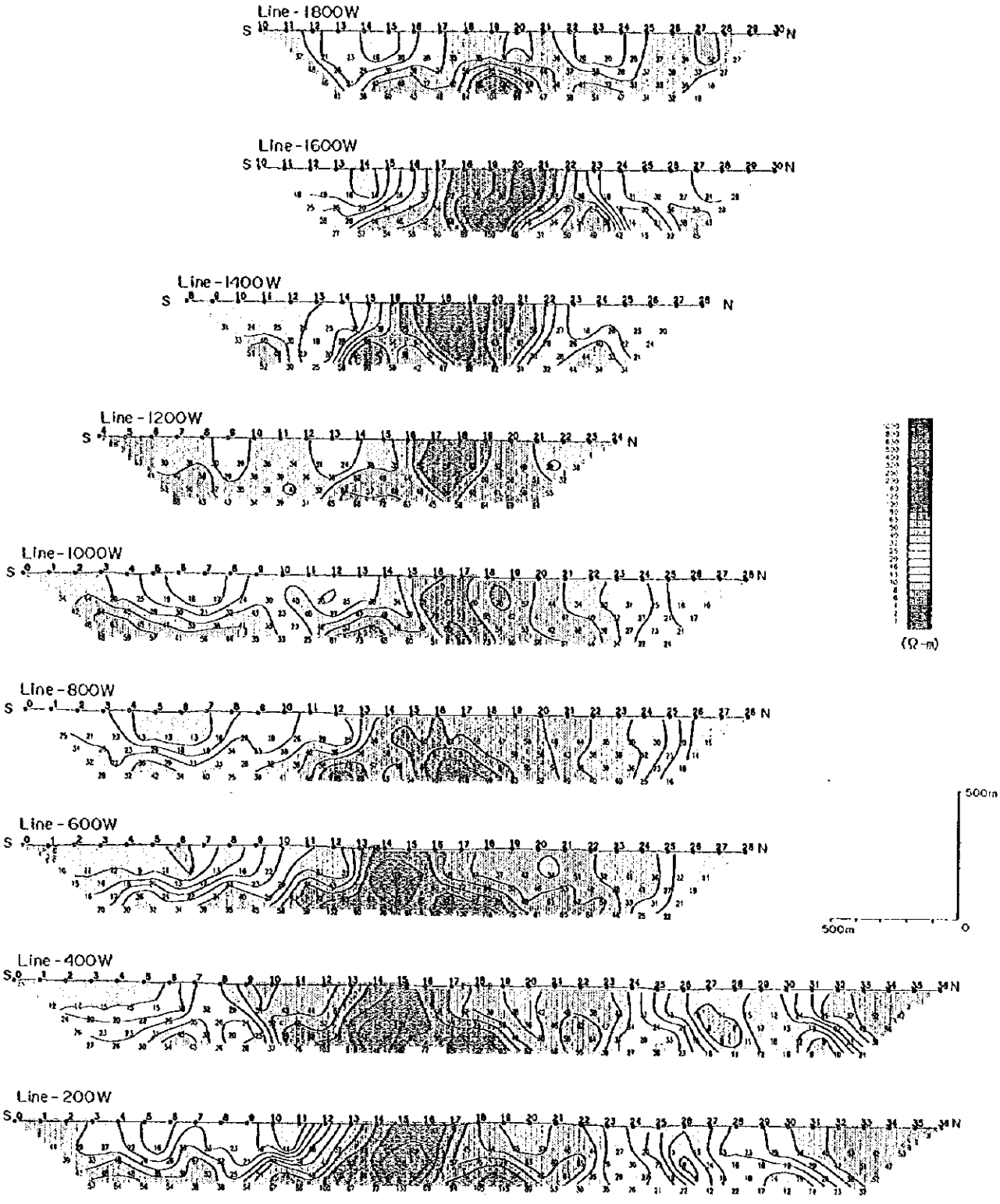

Fig. II-4-41 Apparent resistivity pseudo-sections in Daris area(1)

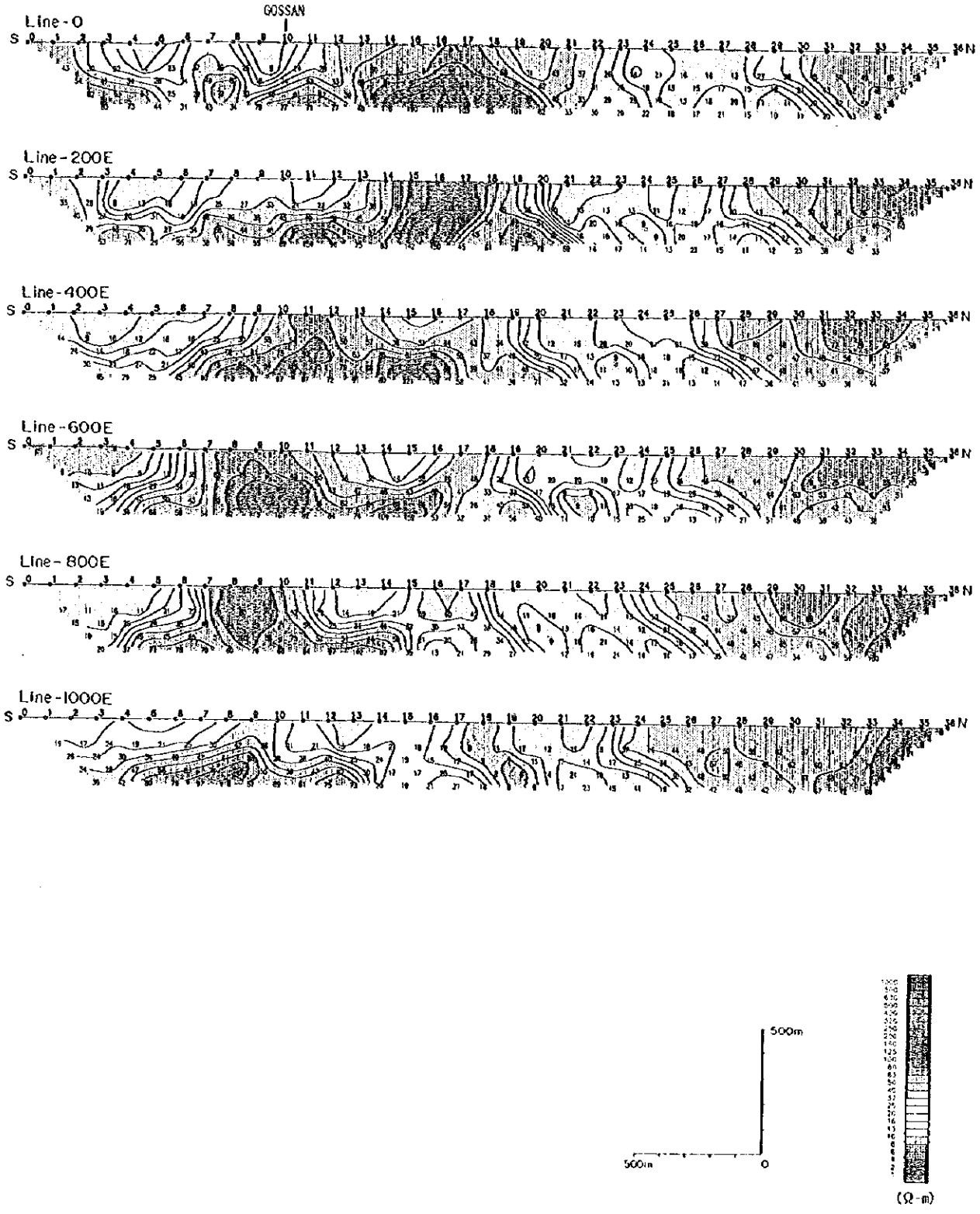

Fig. II-4-42 Apparent resistivity pseudo-sections in Daris area(2)

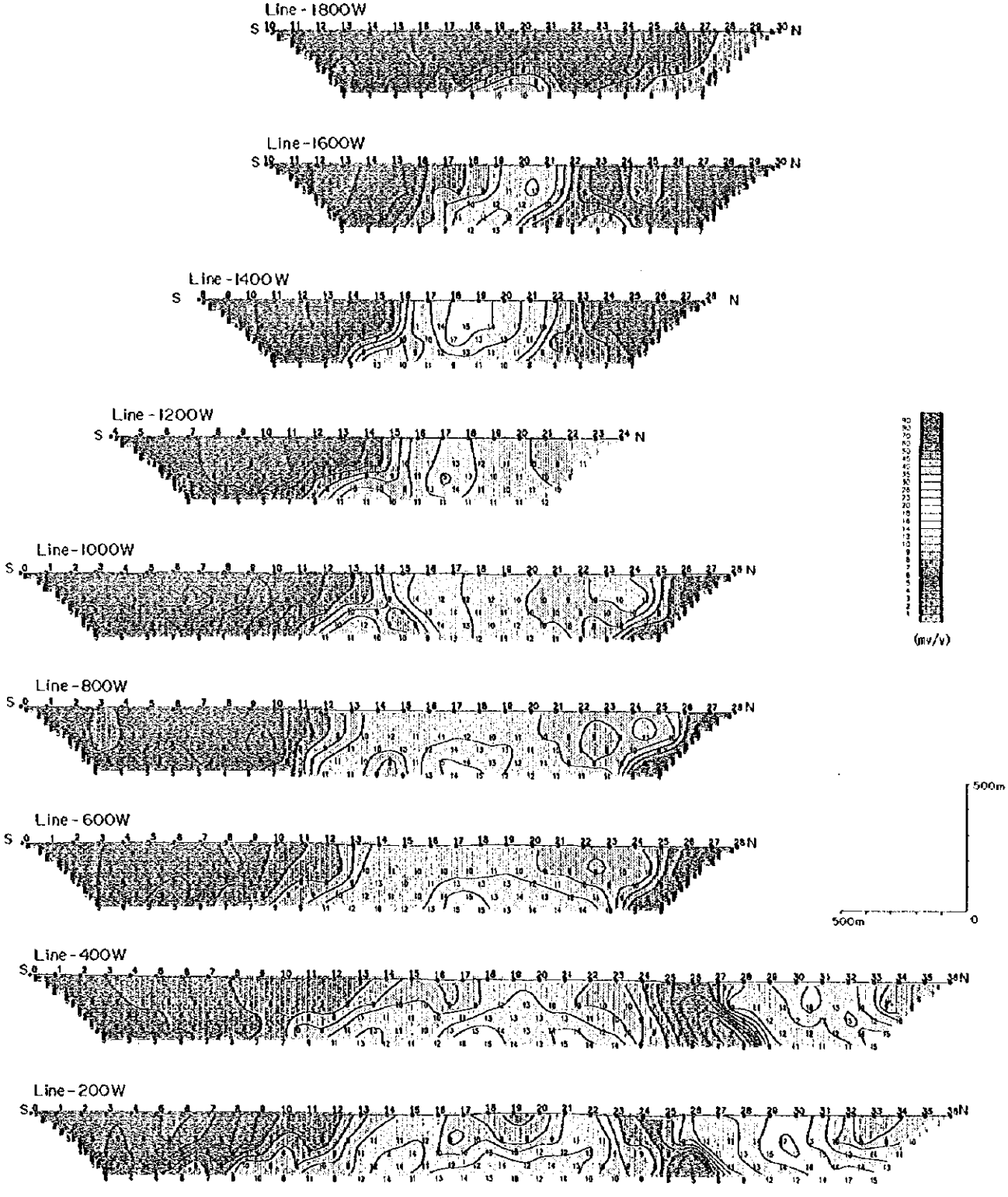

Fig. II -4-43 Chargeability pseudo-sections in Daris area(1)

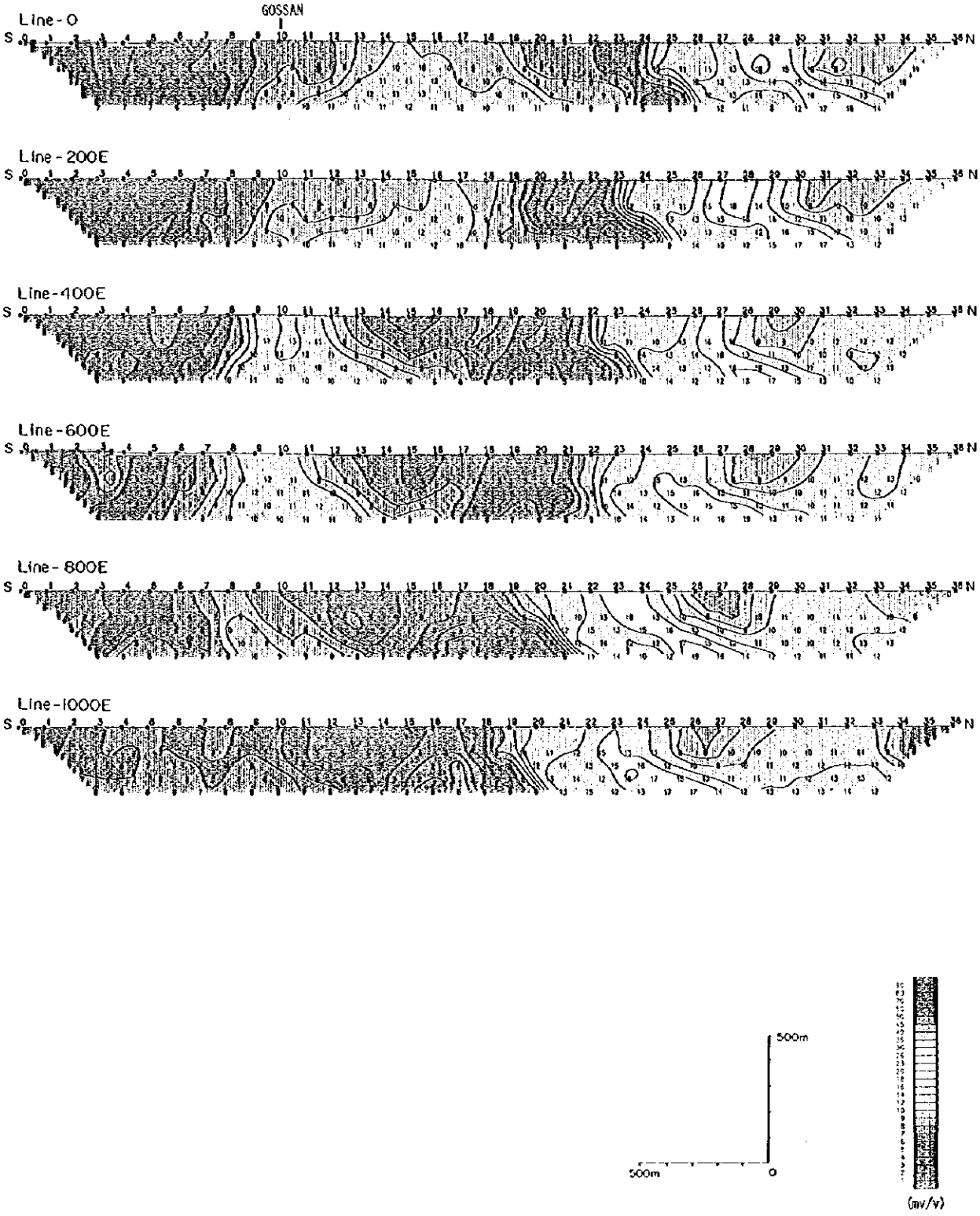

Fig. II-4-44 Chargeability pseudo-sections in Daris area(2)

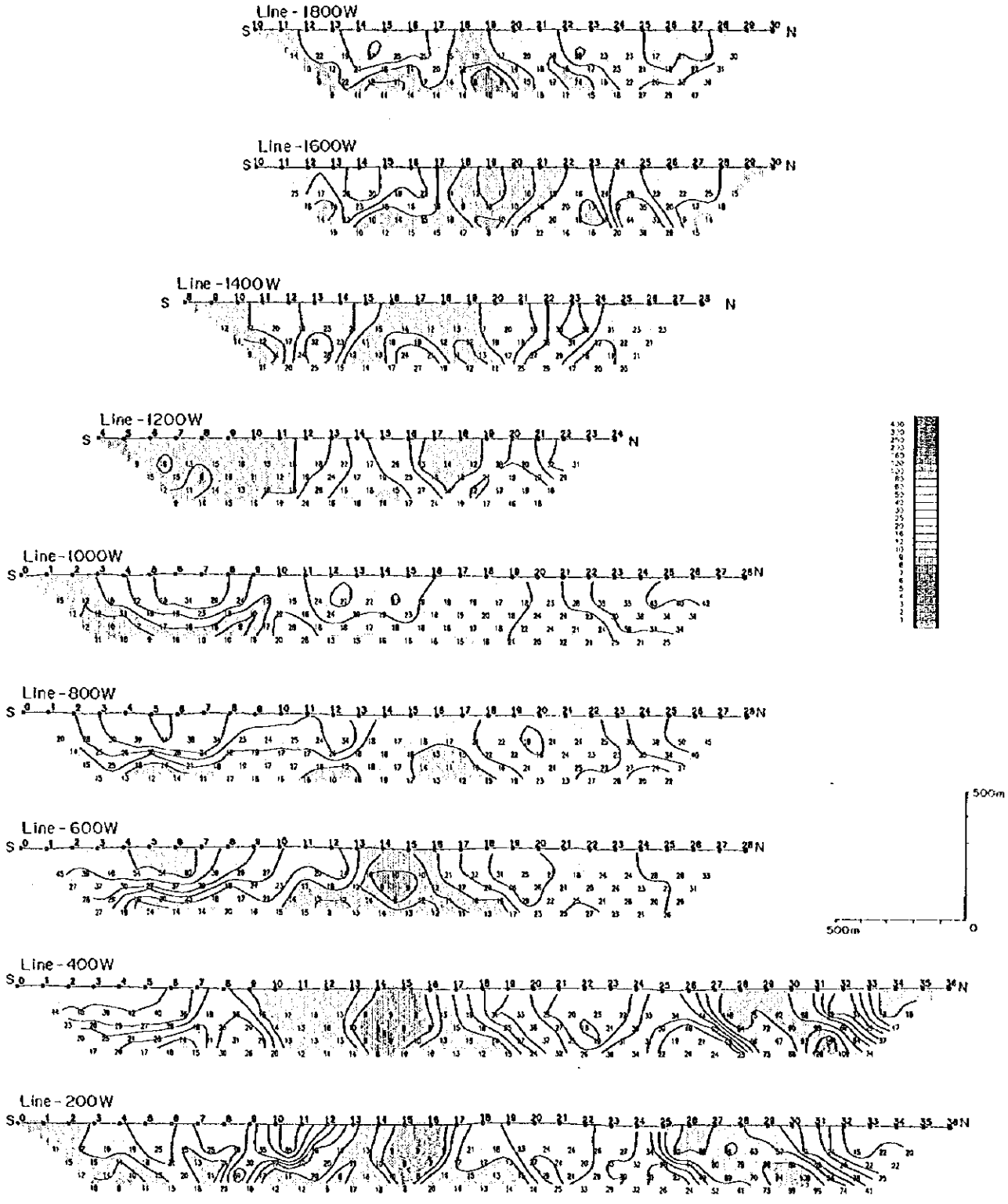

Fig. II-4-45 Metal factor pseudo-sections in Daris area(1)

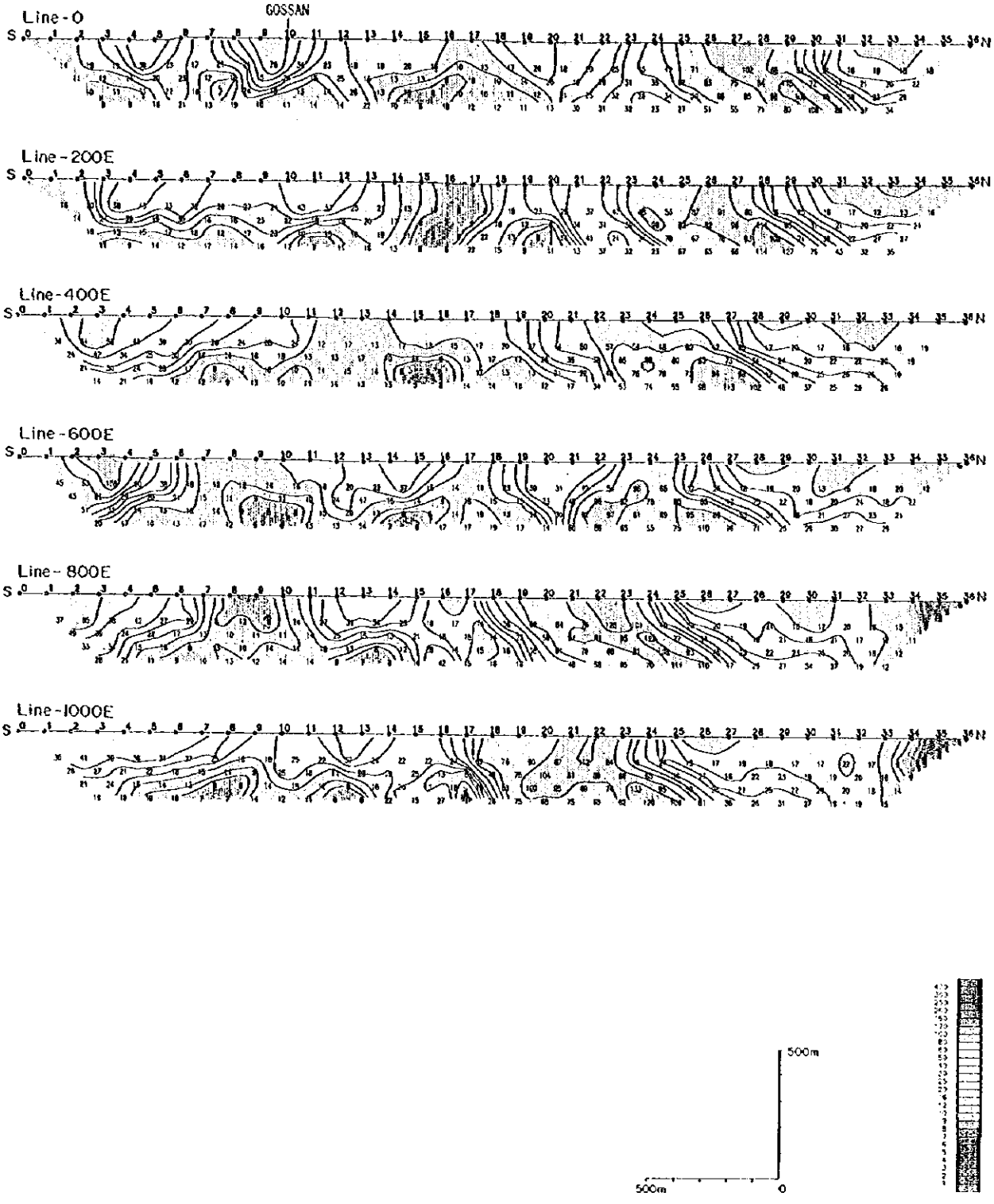

Fig. II-4-46 Metal factor pseudo-sections in Daris area(2)

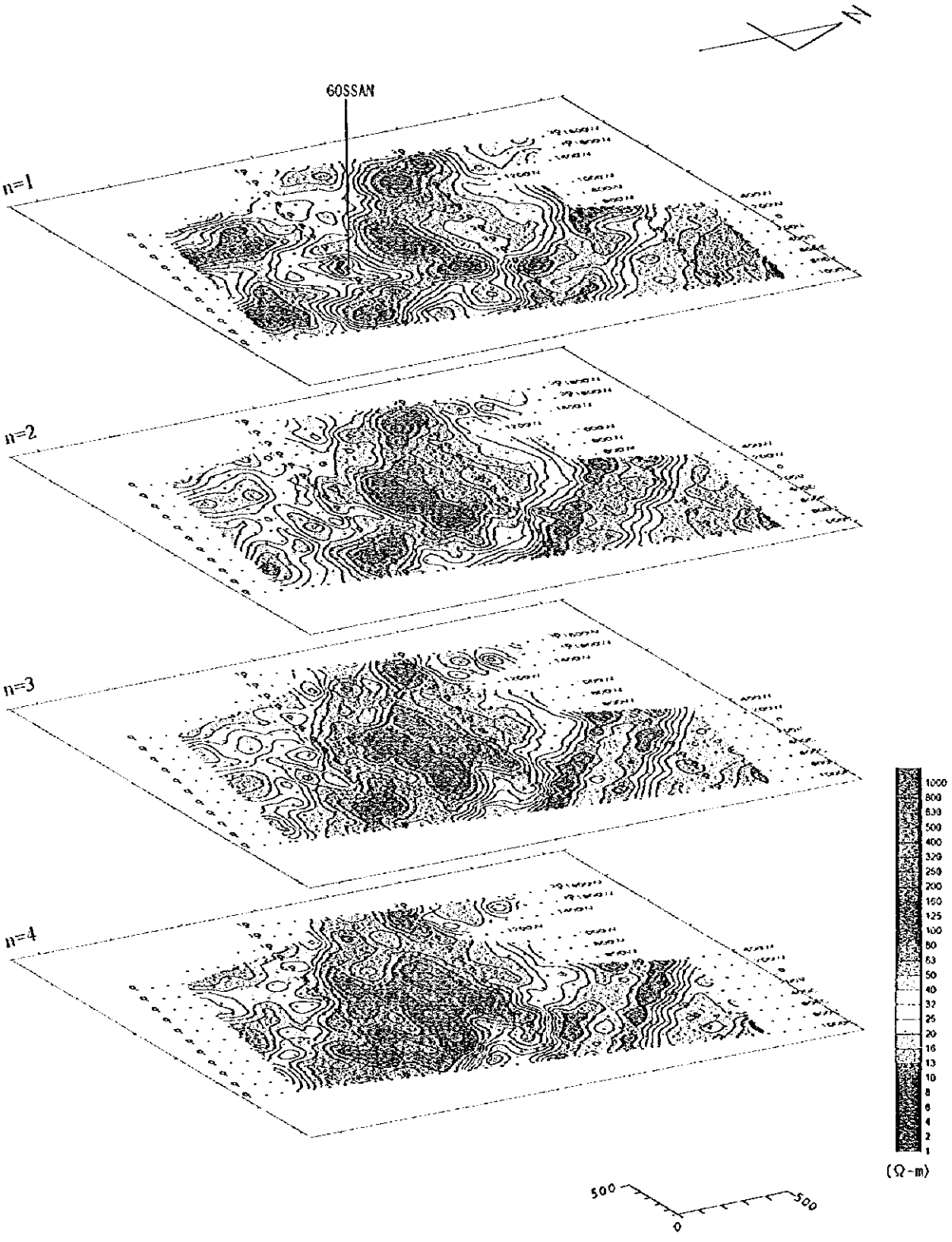

Fig. II -4-47 Apparent resistivity plan map in Daris area

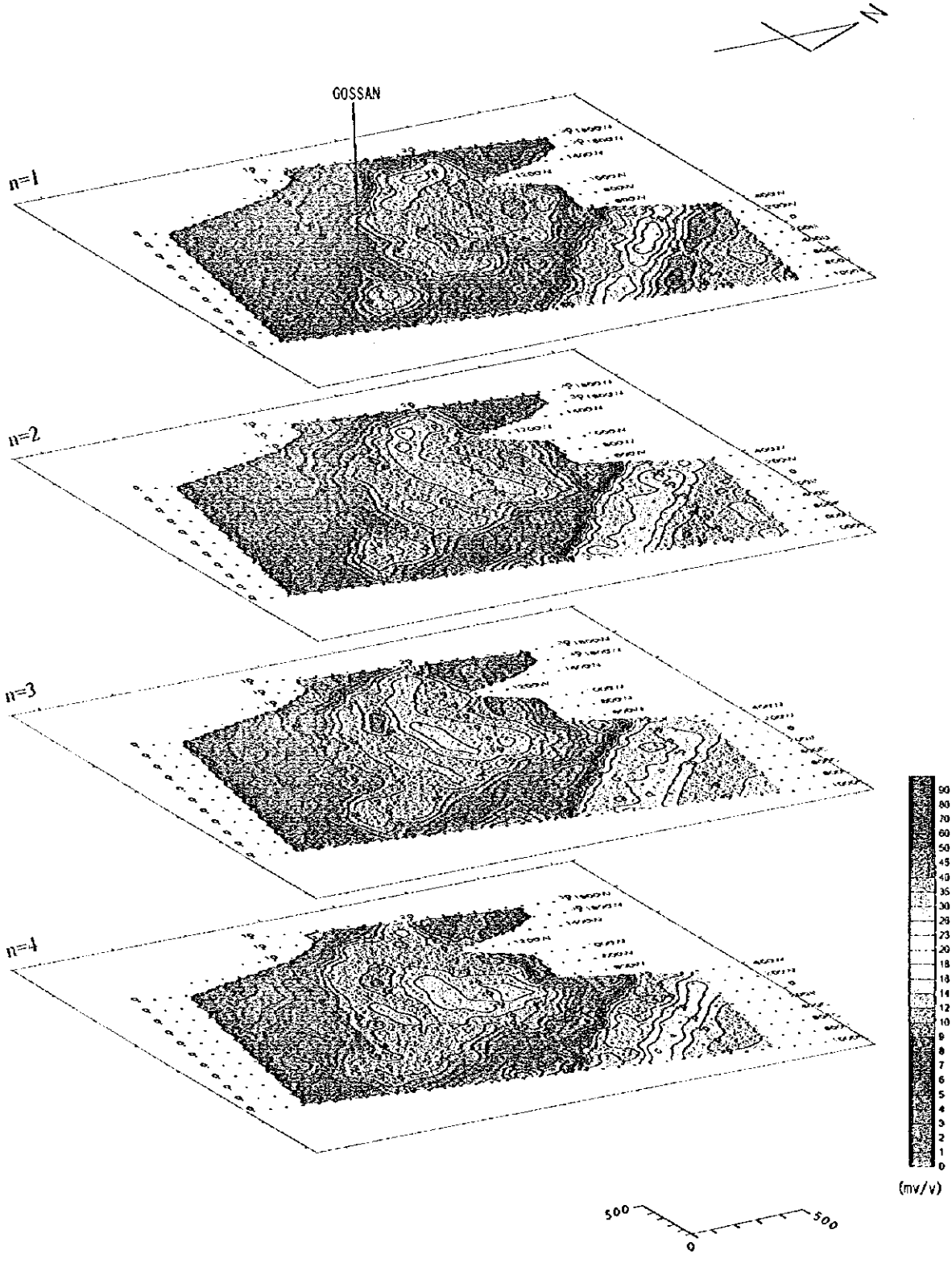

Fig. II-4-48 Chargeability plan map in Daris area

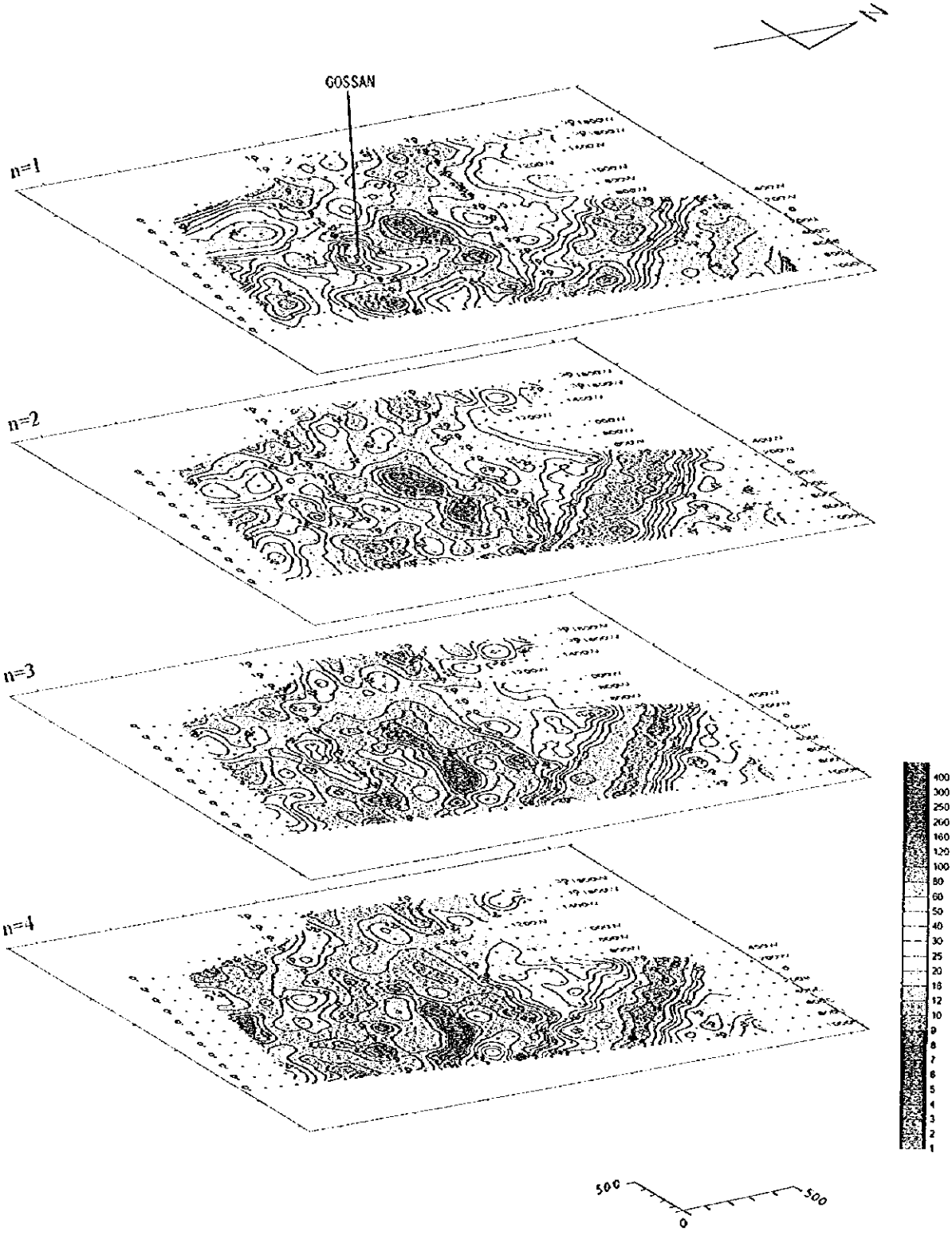

Fig. II-4-49 Metal factor plan map in Daris area

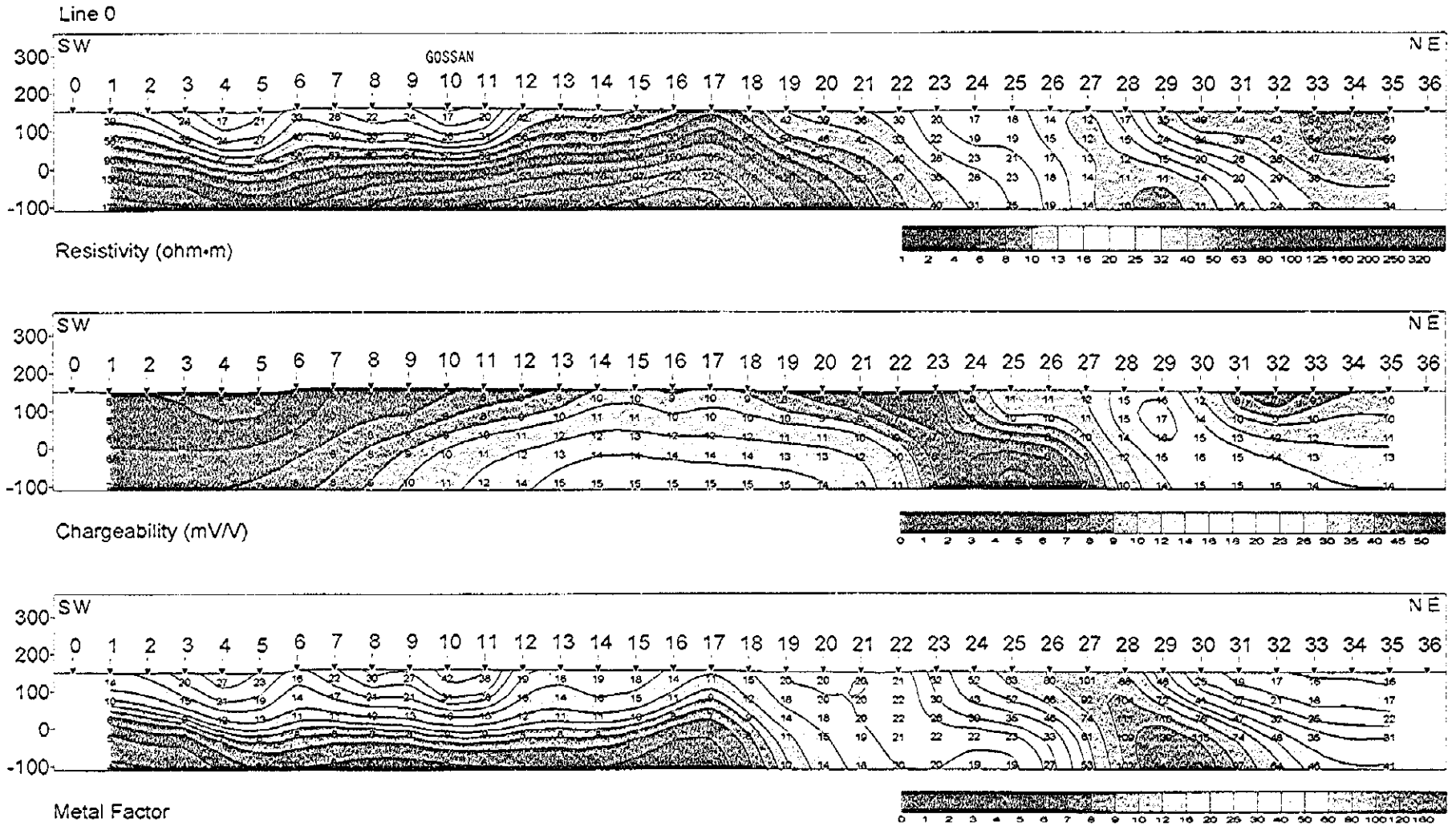

Fig. II -4-50 Results of model simulation in Daris area(1)

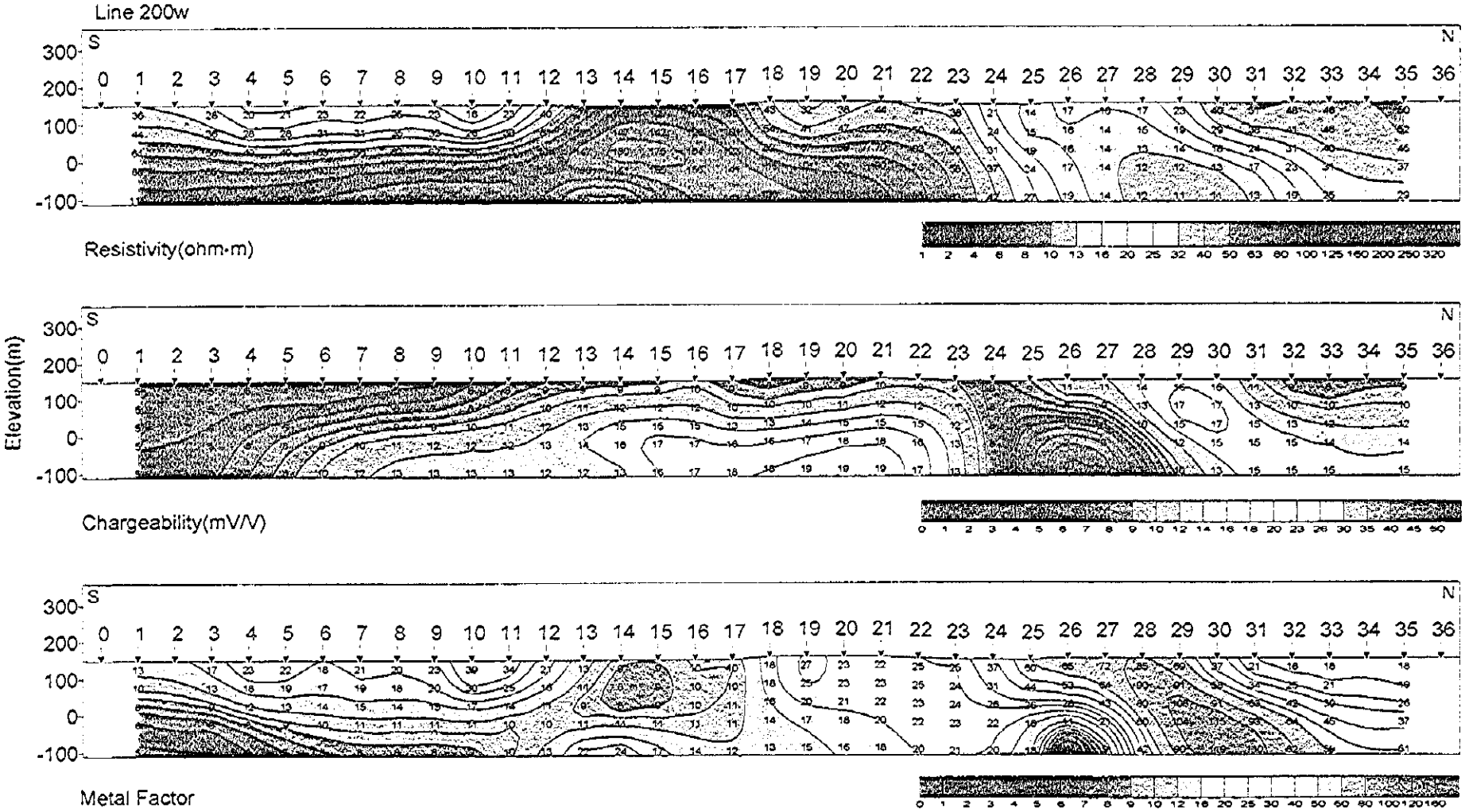

Fig. II-4-51 Results of model simulation in Daris area(2)

CHAPTER 5 TEM SURVEY

5-1 Objectives

The main objective of the TEM survey is to delineate primary massive sulfide zones which contain promising mineralization, based on the results obtained from the time domain IP survey. It is considered that the TEM method is more sensitive than IP to define more conductive zones for delineating possible sulfide-associated mineralizations.

5-2 Survey Locationa and Specifications

Among the five selected survey areas for IP survey, promising anomalies were detected in 2 places in Ghuzayn and 3 in Daris. From them, 3 zones were selected to pursue follow-up TEM geophysical surveys, i.e., 2 in Ghuzayn gossan and 1 in Daris.

The locations of the transmitter loops are indicated in Fig. II-5-1 (Ghuzayn Gossan) and Fig. II-5-2 (Daris). In each of the two areas, TEM measurements were collected within a grid of 400m X 400, making a total of 243 measurement points for both areas.

The amounts of survey carried out in these 2 areas are as indicated in the following Table II-5-1.

Table II-5-1 Survey Amounts

AREA	LOOP SIZE	NUMBER OF POINTS
DARIS	600 X 600 m	81
GHUZAYN GOSSAN N	600 X 600 m	81
GHUZAYN GOSSAN W	600 X 600 m	81
Total		243

5-3 TEM Survey Method

5-3-1 Basic principles

The principle of of the TEM system used in this survey is to energize an ungrounded loop situated on the surface of the earth. When the currents flowing in the loop are switched off, free electron conduction currents are induced (called eddy currents) in the ground. The eddy currents are known to depend on the

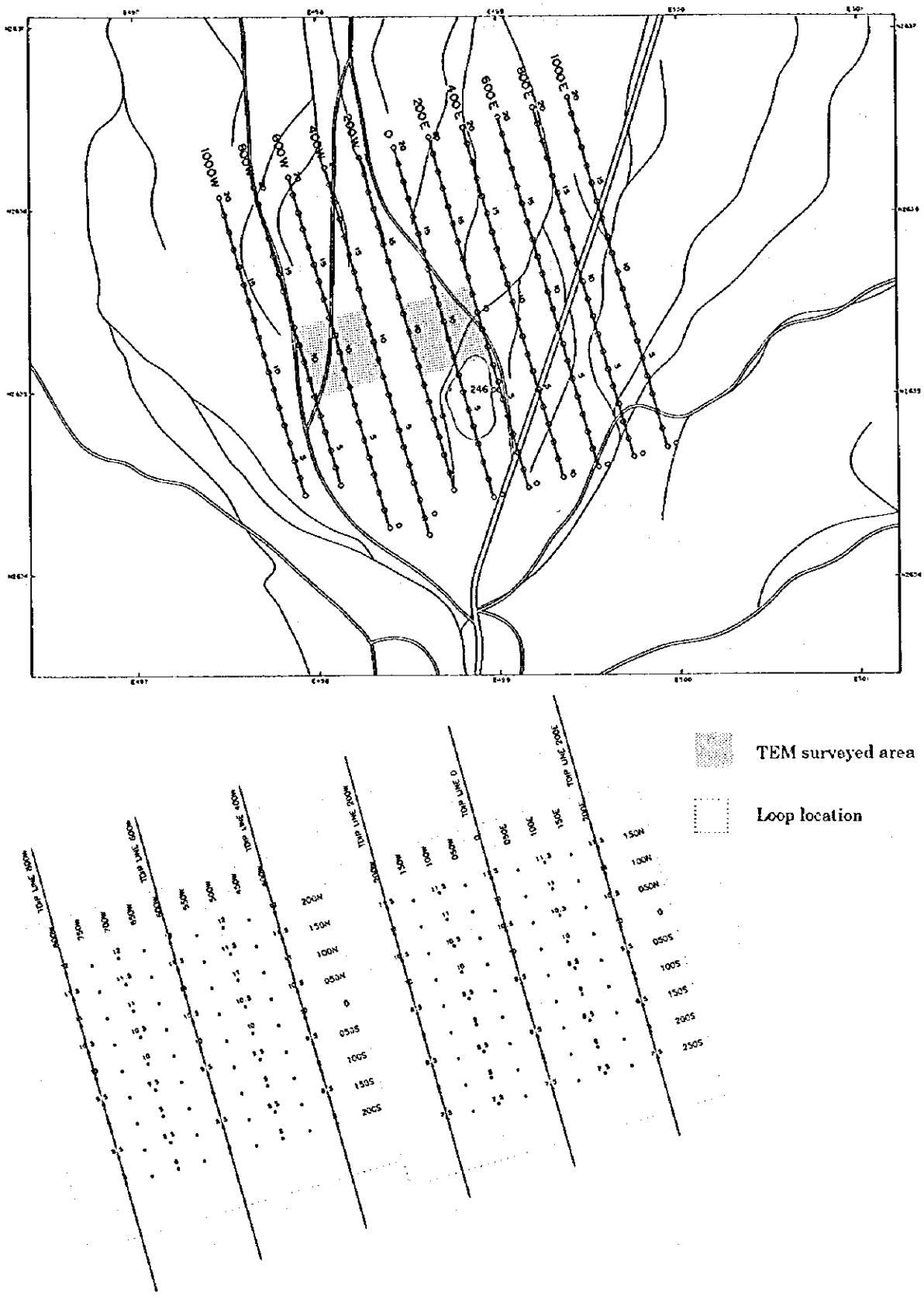

Fig.II-5-1 Ghuzayn survey site showing transmitter loop location

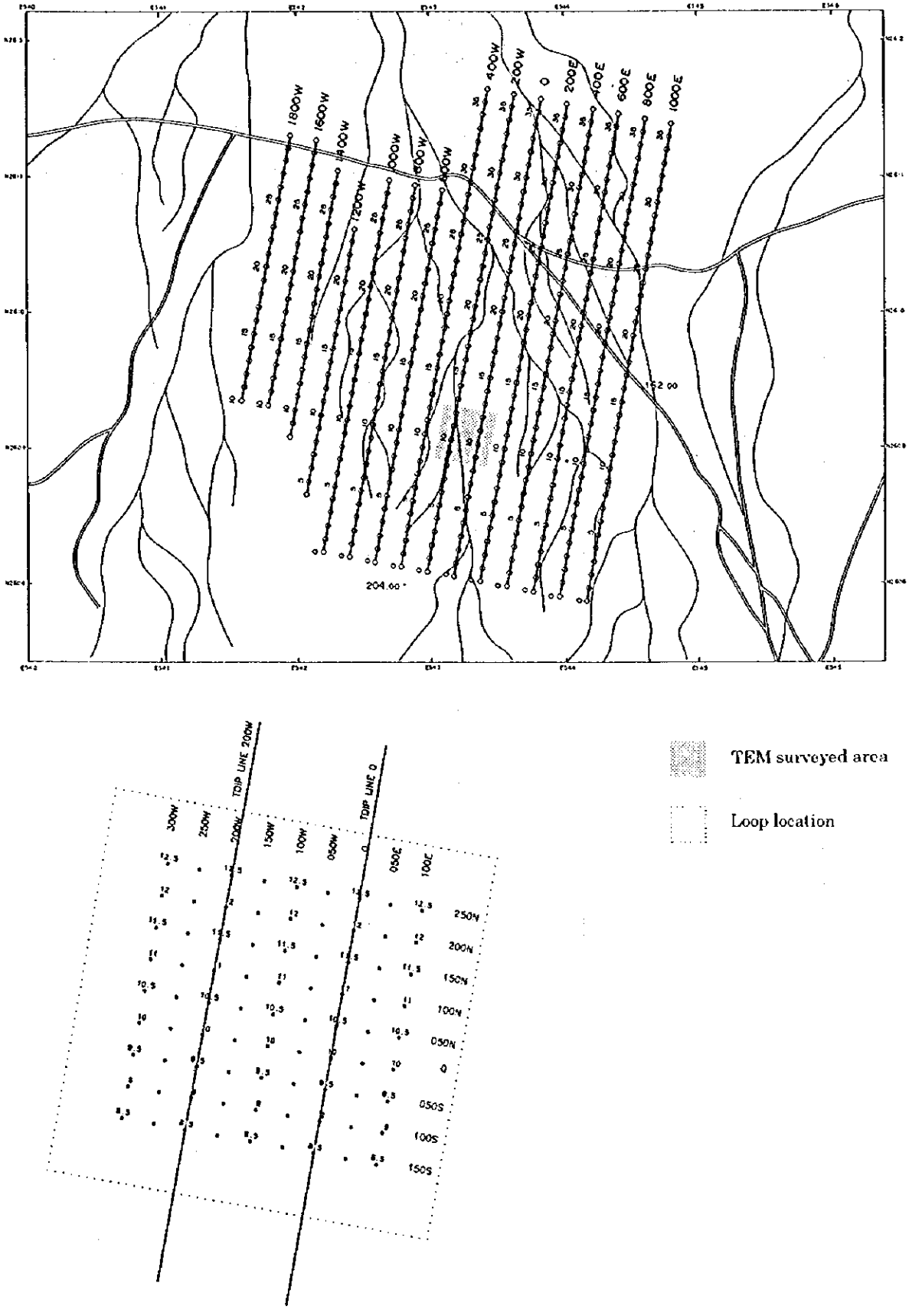

Fig.II-5-2 Daris survey site showing transmitter loop location

conductivity, size and shape of the conducting body, and position with respect to the sensing loop. These eddy currents set up a secondary magnetic field which can be detected by a receiver loop as a time-dependant decaying voltage. Figs. II-5-3

The measurement of the time dependant decaying voltage is a means of detecting conductors in the ground. This decay can be measured by a number of measurement channels recording the voltage at various delay times when the transmitted fields are switched off. Table II-5-2

Table II-5-2 Channel times after switch-off

CHANNEL	GATE CENTER (μsec)	GATE WIDTH (μsec)
1	88	18
2	110	24
3	140	37
4	177	36
5	220	50
6	280	72
7	355	76
8	443	100
9	564	142
10	713	156
11	881	180
12	1096	250
13	1411	380
14	1795	390
15	2224	500
16	2850	720
17	3600	780
18	4490	1080
19	5700	1420
20	7190	1560

The quick decay of the primary magnetic field, caused by the current termination, induces a pulse of electro magnetic force (emf) in the surrounding media, according to Faraday's law. The resulting eddy

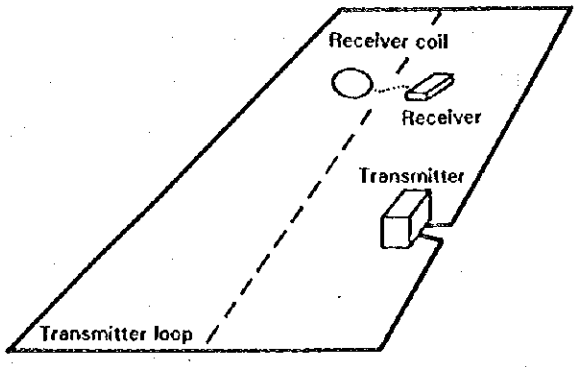

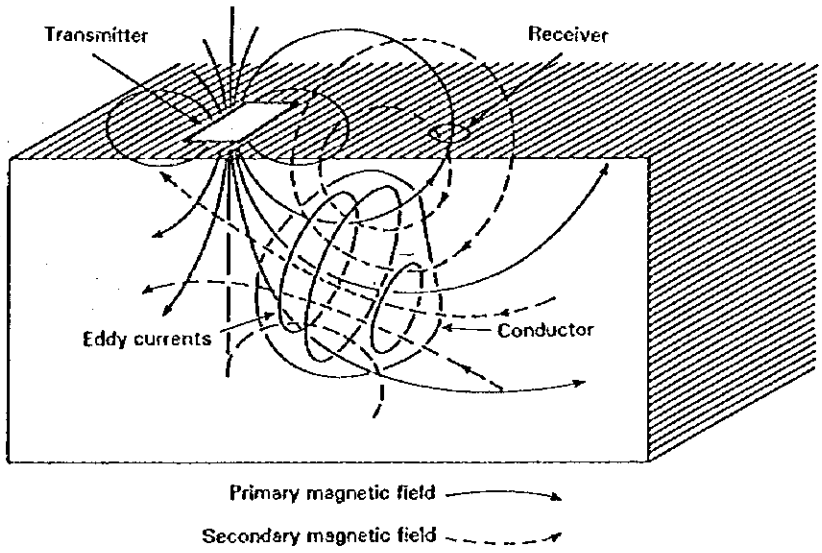

Fig II-5-3 Schematic TEM survey configuration

currents produced in nearby conductive material support a surrounding secondary magnetic field for the duration of the pulse. Thereafter, with no external emf to support it, this system of currents and magnetic field decays with time, and it is this transient magnetic field which the receiver measures. These measurements occur during fixed time "windows" which occupy most of the "off-time" of the transmitter. Since the receiver must know when the transmitter is off, synchronization was done by using crystal clocks.

5-3-2 Survey procedure

There are several varieties of TEM systems and modes of operations. During this survey it was used the fixed-loop TDEM system, in which a large, single-turn loop of wire is laid out on the ground. The loop used was a square loop of 600 m X 600 m carrying about 12 amps. A portable power generator of 2500 W fed a transmitter, which provides a series of alternating bipolar currents pulses with slow exponential turn-on and a rapid linear turn-off precise current waveform through the loop. After the transmitter loop has been set up, a small portable multi-coil receiver is moved to stations inside the loop. the receiver apparatus is moved along surface lines. Lines were surveyed within the loop to a distance of 100m away from the loop and the grid interval between the observed points was 50m. Previous to the data gathering, the crystals of the transmitter and receiver are warmed up before attempting to synchronize. Synchronization of the transmitter and receiver was carried out using the built-in high stability quartz crystal oscillators. Integration for each measurement was carried out over 2^8 cycles.

The current waveform driven through the transmitter loop, and the number of spacing of channels in the receiver are the main distinguishing features of this method. 20 time channels with locations and width are shown in Table 1. Succesive operations at 25Hz, then 2.5Hz, effectively gives 30 channels covering range from 80 μsec. to 71.9 msec (Fig. II-5-4). A steady current is terminated rapidly by a linear ramp

5-3-3 Equipment specifications

The EM37 system is a ground transient EM system manufactured by Geonics Ltd. of Canada.

according to the following specifications:

(1) EM37 transmitter

Although the size of the EM37 transmitting loop can be varied, a single loop of 600 X 600 m was chosen for this survey.

For the loop size we used No. 6.5mm copper wire and a current amplitude of about 12 Amp.

The current waveform in the transmitter consists of alternating bipolar current pulses with a slow exponential turn-on and a rapid linear turn-off. The base frequency of operation can be set at 2.5, 6.25 or 25 Hz, with corresponding window times of 71.9, 28.7 or 7.19 ms respectively. In this survey it was used a base frequency of 25 Hz.

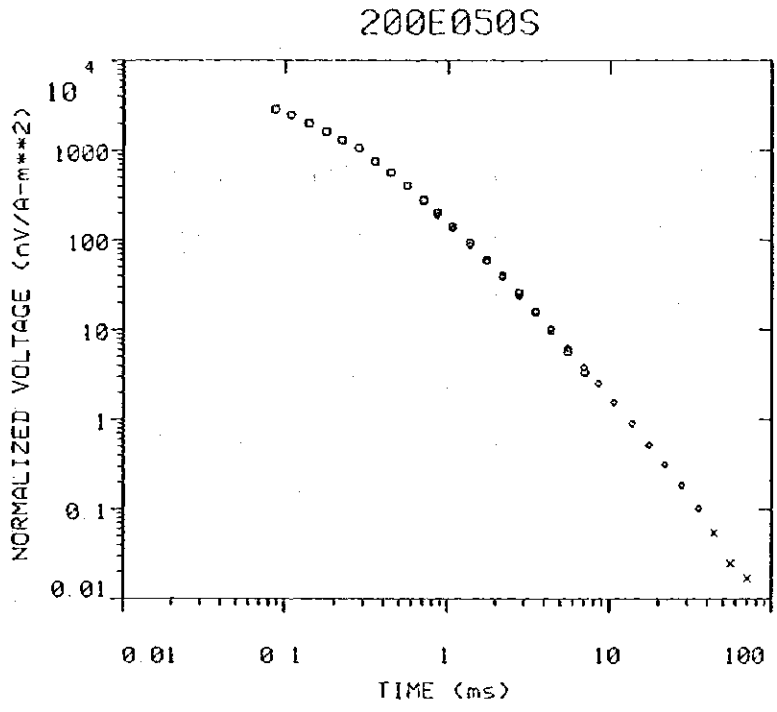

Fig.II-5-4 Example of TEM decay curve

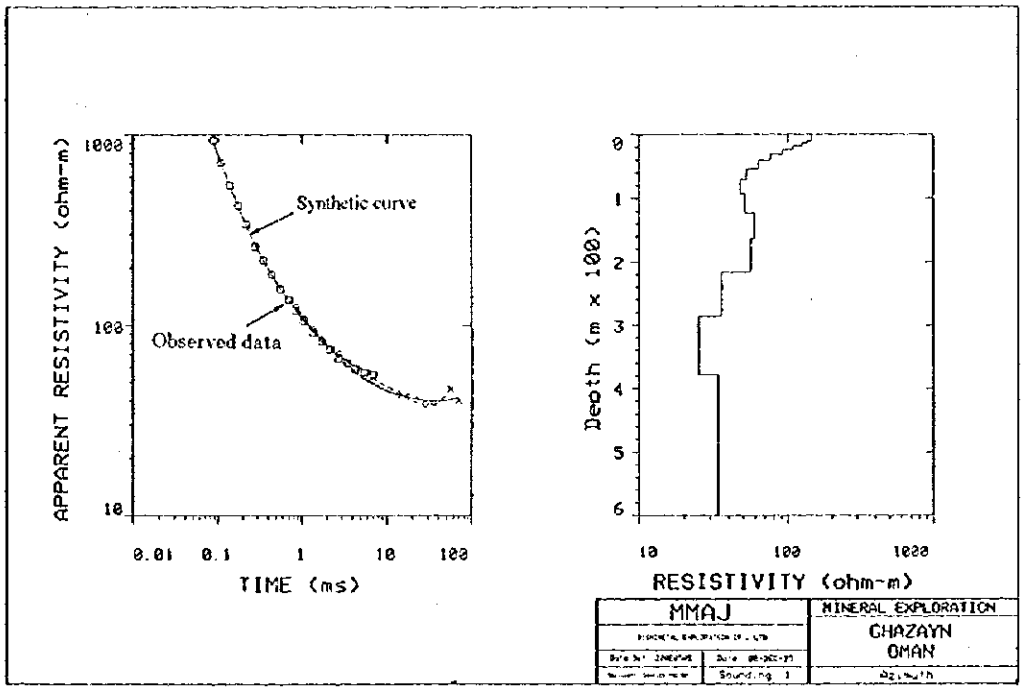

Fig.II-5-5 Example of 1-D smooth layer inversion analysis

Table II-5-3 Instruments

ITEMS	SPECIFICATION
Transmitter	Max. output 30A, 180V
Generator	5HP, 120V, 3phase, 400Hz
Receiver	25.0Hz: 0.88 - 7.19 msec 6.25Hz: 0.35 - 28.7 msec 2.5 Hz: 0.88 - 71.9 msec
Magnetic sensor	Induction coil Effective area: 100 m^2
Recorder	Model DAS54, 500kb

(2) EM37 receiver

Measured quantity : Time rate of decay of magnetic flux

Coil Sensor : Air-cored coil of bandwith 40 kHz; 100cm dia. by 7X5cm cross-section

Time Channels : 20 with locations and width as shown in Table II-5-2

Syncronization to Tx: Oven controlled quartz crystals

Receiver Battery : 12 volt rechargeable Gel-cell.

Station spacing : 50m

At the receiver the induced voltage in the coil is measured in millivolts. Using the effective area of the coil and the gain of the receiver, these measurements are converted to the time derivative of the magnetic field in nanovolts/meter2.

5-4 Analysis Method

The fact that the primary field is absent during measurement time, leads to "cleaner" data which is easier to interpret. The rate of decay of a conductor's magnetic field depends primarily on its size and conductance. Eddy currents decay rapidly in poor conductors, while those due to good conductors decay slowly, and the timing of the channels is such that only the effects of eddy currents due to the good conductors are seen in the later channels. In conductive environments, therefore, the response from overburden and uneconomic ore deposits should be minimal in the later channels where the target response predominates.

After preliminary processing, several of the most useful procedures are:

1. Contour maps of the TEM response for several delay times (windows) in the surveyed area.
2. Time decay plots.
3. TEM profiles, in which the amplitude of the field response is plotted against horizontal distance or station location for a specified time.
4. TEM analyzed profiles, in which the interpreted resistivity is plotted against distance.

The final interpretation of the electromagnetic field data is performed by means of a group of interactive, graphically oriented, forward and inverse modeling programs for interpreting TEM data in terms of a layered earth (1-D) model.

The general procedure for calculating a layered model involves: designing a starting model, performing a forward calculation on the starting model, edit the starting model and performing one or more inverse calculations to achieve a best-fit model for the data.The starting statified model for the case of smooth modeling includes 15 layers with fixed thickness and uniform resistivities, from which synthetic values of the earth resistivity models are obtained.The inversion analysis is based in a ridge regression inversion algorithm to adjust the model parameters, minimizing the least squares error between the data and the synthetic curve (Fig. II-5-5)

The above procedures are complemented by smooth modeling which is used in practice as an alternative presentation of the data or as guide to estimating the starting layered model for inversion. By this method, transient sounding data are interpreted in terms of a smooth model with up to 15 layers by using either ridge regression or Occam's method.

As a result of the inverted 1-D soundings for successive stations, they were compiled from succesive inversion models to give 2-D resistivity sections for each line.

5-5 Ghuzayn Gossan Area

5-5-1 Loop locations

According to the results of the TDIP method, IP anomalies were detected to the north side of the gossan (station 6 line 0) and to the west side of the gossan (line 400). On this basis and to clarify in more detail the nature of these anomalies, the TEM survey method was carried out over these anomalies by using two loops located as indicated in Fig. II-5-1. For the 2 loops, the TEM data were collected within a 400 X 400 grid. Prior to the surveying, one borehole was drilled within the survey area.

5-5-2 Results

(1) Gossan north

The inverted 1-D soundings for all the 81 stations measured in this area, were compiled and as a result, 2-D resistivity sections were obtained for all the 9 lines measured. The compiled 2-D resistivity sections are shown in Fig. II-5-6.

The analysis of the resistivity sections is based here on 4 resistivity layers that can be seen distributed in the area, which from surface to depth, show the following layer structure: a high resistivity structure of resistivity values higher than 100 Ω-m, a low resistivity structure between 20 to 50 Ω-m, a medium-to-high resistivity layer structure with values above 50 Ω-m, and a low resistivity of about few tens of Ω-m.

The first layer structure is in general thin with a thickness of a few tens of meters.

According to the Fig. II-5-7(1) a slightly thick layer of 50 to 75 m are seen distributed in the SE and SW of the area, however in the north edge of the gossan (station 7.5 of line 0) this layer is not seen and instead, the conductive second layer is seen to outcrop. The second layer (low resistivity) presents a maximum thickness of about 50m, however, the depth of the upper surface of the layer gradually becomes deeper towards the north (see line 0 in Fig. II-5-6) and extended towards the north west.(Fig. II-5-7(1)).

The upper surface of the third layer is located about 100m depth and it is distributed widely in the survey area, however, is not seen in the south east area and instead, a low resistivity layer exist at the same depth (Lines 150E, 200E of Fig. II-5-6).

The fourth layer is the deepest among the 4 analyzed layers and seen consistently distributed at a depth deeper than 200m.

(2) Gossan west

The analysis of the resistivity structure in this area takes also into consideration the existence of 4 resistivity layers that can be seen distributed in the area, which from surface to the depths show the following layer structure: high resistivity structure of with resistivity values higher than 100 Ω-m, a low resistivity structure between 10 to few tens of 50 Ω-m, a medium-to-high resistivity of values above 50 Ω-m, and a low-to-medium resistivity between 20 to few tens of Ω-m (Fig. II-5-8).

The thickness of the first layer is less than 50m and is generally thin, but becomes thicker in the NW and center of the south part of the area as seen in the resistivity plan map at the depth of 50m show in the Fig. II-5-9(1).

The low resistivity structure of the second layer shows a thickness of several tens meters and distributed uniformly which as seen, for instance in lines 450W and 500W (Fig. II-5-8), show resistivity values as low as 10 to 13 Ω-m. This layer gradually gets deeper toward the west and at the same time, the resistivite values become higher. The third layer structure of medium to high resistivity is seen distributed